# Final Report: Investigation of subgrid-scale mixing and turbulence-chemistry interaction in turbulent partially premixed flames

AFOSR Grant F-9550-06-1-0036

Principal Investigator: Chenning Tong

Department of Mechanical Engineering
Clemson University
Clemson, SC 29634-0921

## I Introduction

This research project focused on issues met in using large-eddy simulation (LES) to predict turbulent nonpremixed combustion. LES has been recognized as a very promising approach to modeling such flames[1, 2, 3]. In this approach the subgrid-scale (SGS) scalar mixing and the resulting instantaneous distribution of scalar values in each grid volume (i.e., the filtered density function) must be faithfully represented in order to accurately predict the chemical reaction rate. This research studied issues in using this approach by investigating the SGS mixing of mixture fraction and temperature using experimental data obtained in turbulent partially premixed (Sandia) flames. The former is a conserved scalar whereas the latter is a reactive scalar. Therefore, the present study provides an understanding for mixing models to treat SGS mixing of both conserved and reactive scalars. Specifically, the following work was completed:

- Investigated the filtered mass density function of (FMDF) the mixture fraction using experimental data. The FMDF and the structure of the SGS scalar were found to strongly depend on the SGS variance (degree of nonequilibrium spectral transfer).
- Investigated the conditionally filtered scalar dissipation rate which is the most important term in the transport equation of of the FMDF of the mixture fraction. The results were found to depend strongly on the degree of nonequilibrium spectral transfer.
- Investigated the filtered mass density function of the mixture fraction and temperature using experimental data.

# REPORT DOCUMENTATION PAGE

*Form Approved*
*OMB No. 0704-0188*



| **1. REPORT DATE** *(DD-MM-YYYY)* | **2. REPORT TYPE** | **3. DATES COVERED** *(From 15-11-2005 To 14-11-2008)* |
|---|---|---|
| 13-02-2009 | Final Report | |

**4. TITLE AND SUBTITLE**
[U] Investigation of subgrid-scale mixing and turbulence-chemistry interaction in turbulent partially premixed flames

**5a. CONTRACT NUMBER**

**5b. GRANT NUMBER**
F-9550-06-1-0036

**5c. PROGRAM ELEMENT NUMBER**
61102F

**6. AUTHOR(S)**
Chenning Tong

**5d. PROJECT NUMBER**
2308

**5e. TASK NUMBER**
BX

**5f. WORK UNIT NUMBER**

**7. PERFORMING ORGANIZATION NAME(S) AND ADDRESS(ES)**

Department of Mechanical Engineering
Clemson University
Clemson, SC 29634

**8. PERFORMING ORGANIZATION REPORT NUMBER**

**9. SPONSORING / MONITORING AGENCY NAME(S) AND ADDRESS(ES)**
AFOSR/NA
875 Randolph Street
Suite 325, Room 3112
Arlington, VA 22203

**10. SPONSOR/MONITOR'S ACRONYM(S)**

**11. SPONSOR/MONITOR'S REPORT NUMBER(S)** AFRL-SR-AR-TR-09-0158

**12. DISTRIBUTION / AVAILABILITY STATEMENT**

Approved for public release, distribution unlimited

**13. SUPPLEMENTARY NOTES**

**14. ABSTRACT**

This research project focused on issues met in using large-eddy simulation (LES) to predict turbulent nonpremixed/partially premixed combustion. In LES of such flames the subgrid-scale scalar mixing and the resulting subgrid-scale scalar distributions must be faithfully represented. In this research the mixture fraction filtered mass density function (FMDF) and the FMDF of mixture fraction and temperature were studied experimentally using data from Sandia flames. The results show that the subgrid-scale mixture fraction has two limiting distributions and structures, which have strong effects on the flame structure. The SGS fields with small and large SGS variance the scalar and temperature dissipation structures were consistent with those in quasi-equilibrium distributed reaction zones and strained laminar flamelets, respectively. For small SGS variance the scalar and temperature diffusion had a simple structure whereas for large SGS variance the diffusion structure was much more complex, with the pilot and local extinction also playing important roles. The results in the present study suggest that it is important for combustion models to predict both distributed reaction zones and flamelets as well as their extinction. Specifically, mixing models need to be able to account for the different SGS temperature structures and the SGS mixing time scales resulted from the different SGS mixture fraction structures.

**15. SUBJECT TERMS**

| **16. SECURITY CLASSIFICATION OF:** | | | **17. LIMITATION OF ABSTRACT** | **18. NUMBER OF PAGES** | **19a. NAME OF RESPONSIBLE PERSON** |
|---|---|---|---|---|---|
| **a. REPORT** | **b. ABSTRACT** | **c. THIS PAGE** | UL | 41 | Julian M. Tishkoff |
| Unclassified | Unclassified | Unclassified | | | **19b. TELEPHONE NUMBER** *(include area code)* 703 696-8478 |

- Investigated the conditionally filtered scalar dissipation rate and temperature dissipation rate conditional on both mixture fraction and temperature, which are the most important terms in the transport equation of the FMDF of mixture fraction and temperature. The effects of the SGS mixture fraction structure on the SGS flame structure were studied.
- Developed and tested a conditional-sampling-based method for noise and resolution corrections for scalar dissipation rate measurements. Applied the method to turbulent partially premixed flames. This method is the first to make use of the unique property of the turbulent scalar fields, allowing high accuracy corrections even for highly noisy signals.

The primarily findings of this research are discussed in the following.

# II Nomenclature

| | |
|---|---|
| $\xi$ | mixture fraction |
| $\hat{\xi}$ | sample-space variable for mixture fraction |
| $T$ | temperature |
| $\hat{T}$ | sample-space variable for temperature |
| $F_{\xi L}(\hat{\xi};\mathbf{x},t)$ | mixture fraction filtered mass density function (FMDF) |
| $\chi$ | scalar dissipation rate |
| $\chi_T$ | temperature dissipation rate |
| $D$ | molecular diffusivity or jet diameter |
| $F_{\xi T L}(\hat{\xi},\hat{T};\mathbf{x},t)$ | FMDF of mixture fraction and temperature |
| $\langle\xi\rangle_L$ | Favre filtered mixture fraction |
| $\langle\xi''^2\rangle_L$ | Favre subgrid-scale scalar variance |
| $\Delta$ | filter size |
| $n$ | measurement noise |
| $h$ | sample spacing |

$C_N$ scheme dependent coefficient in noise estimation

# III Findings

The mixture fraction FMDF is defined as

$$F_{\xi L}(\hat{\xi};\mathbf{x},t) = \langle \rho(\mathbf{x},t)\delta(\xi-\hat{\xi};\mathbf{x},t)\rangle_\ell = \int \rho(\mathbf{x}',t)\delta(\xi-\hat{\xi};\mathbf{x}',t)G(\mathbf{x}-\mathbf{x}')d\mathbf{x}', \tag{1}$$

where $\xi$, $\rho$, and $G$ are the mixture fraction, the fluid density, and the filter function, respectively. The subscripts $\ell$ and $L$ denote conventional and Favre filtered variables, respectively. The FMDF transport equation is

$$\frac{\partial F_{\xi L}}{\partial t} + \frac{\partial}{\partial x_j}\{\langle u_j|\hat{\xi}\rangle_L F_{\xi L}\} = \frac{\partial}{\partial x_j}(D\frac{\partial F_{\xi L}}{\partial x_j}) - \frac{\partial^2}{\partial \hat{\xi}^2}\{\langle \chi|\hat{\xi}\rangle_L F_{\xi L}\}, \tag{2}$$

where $\chi = \langle 2D\frac{\partial \xi}{\partial x_j}\frac{\partial \xi}{\partial x_j}|\xi\rangle_\ell$ and $D$ are the scalar dissipation rate and the molecular diffusivity, respectively.

The filtered mass density function function of mixture fraction and temperature is

$$F_{\xi TL}(\hat{\xi},\hat{T};\mathbf{x},t) = \langle \rho(\mathbf{x},t)\delta(\xi-\hat{\xi})\delta(T-\hat{T})\rangle_\ell = \int \rho(\mathbf{x}',t)\delta(\xi-\hat{\xi})\delta(T-\hat{T})G(\mathbf{x}-\mathbf{x}')d\mathbf{x}', \tag{3}$$

where $T$ and $\hat{T}$ are temperature, and its sample-space variables, respectively. The FMDF transport equation is

$$\frac{\partial F_{\xi TL}}{\partial t}+\frac{\partial}{\partial x_j}\{\langle u_j|\hat{\xi},\hat{T}\rangle_\ell F_{\xi TL}\}=$$
$$-\frac{\partial}{\partial\hat{\xi}}\{\frac{1}{\rho}\langle\frac{\partial}{\partial x_j}(\rho D\frac{\partial\xi}{\partial x_j})|\hat{\xi},\hat{T}\rangle_\ell F_{\phi L}\}-\frac{\partial}{\partial\hat{T}}\{\frac{1}{\rho}\langle\frac{\partial}{\partial x_j}(\rho D\frac{\partial T}{\partial x_j})|\hat{\xi},\hat{T}\rangle_\ell F_{\xi TL}\}-\frac{\partial}{\partial\hat{T}}\{s_\alpha(\hat{\boldsymbol{\phi}})F_{\xi TL}\}$$
$$=-\frac{\partial^2}{\partial x_j}(D\frac{\partial F_{\xi TL}}{\partial x_j})-\frac{\partial^2}{\partial\hat{\xi}\partial\hat{T}}\{\langle D\frac{\partial\xi}{\partial x_j}\frac{\partial T}{\partial x_j}|\hat{\xi},\hat{T}\rangle_\ell F_{\xi TL}\}-$$
$$\frac{\partial^2}{\partial\hat{\xi}^2}\{\langle D\frac{\partial\xi}{\partial x_j}\frac{\partial\xi}{\partial x_j}|\hat{\xi},\hat{T}\rangle_\ell F_{\xi TL}\}-\frac{\partial^2}{\partial\hat{T}^2}\{\langle D\frac{\partial T}{\partial x_j}\frac{\partial T}{\partial x_j}|\hat{\xi},\hat{T}\rangle_\ell F_{\xi TL}\}-\frac{\partial}{\partial\hat{T}}\{s_\alpha(\hat{\boldsymbol{\phi}})F_{\xi TL}\},\tag{4}$$

where $\mathbf{s}$ is the reaction rate for temperature, respectively, a function of the species mass fractions and enthalpy $\boldsymbol{\phi}$; $\hat{\boldsymbol{\phi}}$ represents the sample-space variables for $\boldsymbol{\phi}$. The first two terms in the equation are the time rate of change and advection in physical space respectively. The rest of the terms include diffusion of the FMDF in physical space, transport of the FMDF in scalar space by the conditionally filtered mixture fraction diffusion, the conditionally filtered temperature diffusion, the conditionally filtered mixed dissipation, the conditionally filtered mixture fraction dissipation, the conditionally filtered temperature dissipation, and the reaction.

In this research we focused on the FMDF, the mixture fraction dissipation, and the temperature dissipation rate to investigate SGS mixing and turbulence-chemistry interaction. We used experimental data obtained in piloted turbulent partially premixed methane flames with a 1:3 ratio of $CH_4$ to air by volume (Sandia flames D and E, see Ref.[4, 5, 6]). The measurements employed combined line-imaging of Raman scattering, Rayleigh scattering, and laser-induced CO fluorescence. Simultaneous measurements of major species ($CO_2$, $O_2$, CO, $N_2$, $CH_4$, $H_2O$, and $H_2$), mixture fraction (obtained from all major species), temperature, and the radial component of scalar dissipation rate were made. The mixture fraction was calculated using a variation of Bilger's definition, which had been modified by excluding the oxygen terms[4]. In the following we briefly outline the results from our study and their implications for LES.

### A. Scalar filtered mass density function in turbulent partially premixed flames

Unlike a PDF and the conditional dissipation, the FMDF and the conditionally filtered dissipation are random variables. Therefore they were analyzed here using their conditional averages. We used the Favre filtered mixture fraction,

$$\langle\xi\rangle_L=\langle\rho\xi\rangle_\ell/\langle\rho\rangle_\ell,\tag{5}$$

and the Favre SGS scalar variance,

$$\langle\xi''^2\rangle_L\equiv\frac{1}{\langle\rho\rangle_\ell}\int F_{\xi L}(\hat{\xi};\mathbf{x},t)(\hat{\xi}-\langle\xi\rangle_L)^2d\hat{\xi}=\langle\rho\xi^2\rangle_\ell/\langle\rho\rangle_\ell-\langle\xi\rangle_L^2\tag{6}$$

(also random variables) as conditioning variables, which provide a measure of the unmixedness of the mixture fraction. The latter is also an important variable in the inertial-range dynamics, and therefore can relate the FMDF to the inertial-range dynamics. Such a linkage is important for modeling SGS mixing.

The conditional mixture fraction FMDF, $\langle F_{\xi L}|\langle\xi\rangle_L, \langle\xi''^2\rangle_L\rangle$, for flame D at $x/D = 15$ for several SGS variance values is shown in Fig. 1b. The filter scale is $\Delta = 3.0$ mm. We set $\langle\xi\rangle_L$ to the stoichiometric mixture fraction, $\xi_s(= 0.35)$, to maximize the probability of the SGS field containing reaction zones. For small SGS variance, e.g. $\langle\xi''^2\rangle_L \approx 0.0004$, the conditional FMDF is unimodal and generally not far from Gaussian. Such a distribution is similar to those obtained in nonreacting flows and to the scalar PDF in a fully developed turbulent flow, indicating that the SGS mixture fraction was well mixed. Previous results[7, 8] have shown that the SGS scalar under such conditions is in spectral equilibrium and the SGS scalar is consistent with Kolmogorov's cascade picture. Therefore, the average SGS scalar fluctuations decreases with the filter scale, suggesting that the burden on the SGS mixing models is lessened.

As the SGS variance increases, the FMDF becomes bimodal, with the bimodality stronger for larger SGS variance, indicating that the rich and lean mixtures in the SGS field (i.e., a grid cell) were essentially segregated. Furthermore, there was a sharp interface (diffusion-layer) separating the two regions, across which there was a large scalar value jump (see the discussion on the conditionally filtered scalar dissipation rate below). This SGS scalar structure is essentially a ramp-cliff structure (see Ref.[9]), with the rich and lean mixtures forming the ramps and the diffusion layer as the cliff. The bimodal FMDF is also similar to the scalar FDF for large SGS variance observed in nonreacting flows [7]. Our previous results also showed that the SGS scalar with a large variance is in spectral nonequilibrium, which, along with the presence of the ramp-cliff structure, suggests that the bimodal SGS scalar is not well described by Kolmogorov's turbulence cascade picture. Because the ramp-cliff structure exists in the subgrid scales for all filter sizes significantly larger than the Corrsin scale, as is the case in most LES, the burden on mixing models to capture the bimodal FMDF does not lessen with decreasing filter scale.

The value of the Favre filtered mixture fraction has different effects on the unimodal and bimodal conditional FMDFs. For a unimodal FMDF, the shape remains approximately unchanged when $\langle\xi\rangle_L$ increases from 0.35 to 0.45 (Fig. 2a), but the position of the peak shifts rightward to approximately 0.42 (leftward to 0.22 for $\langle\xi\rangle_L = 0.25$, not shown). The close-to-Gaussian distributions indicate that the conditional SGS mixture fraction fields were still well-mixed and diffused toward $\langle\xi\rangle_L$. For $\langle\xi\rangle_L$ values sufficiently away from $\xi_s$, the SGS field might not contain any reaction zones. Therefore, the FMDFs of such fields are of less interest and not shown. For a bimodal FMDF, the positions of the two peaks move much less than that of a unimodal FMDF as $\langle\xi\rangle_L$ increases, but

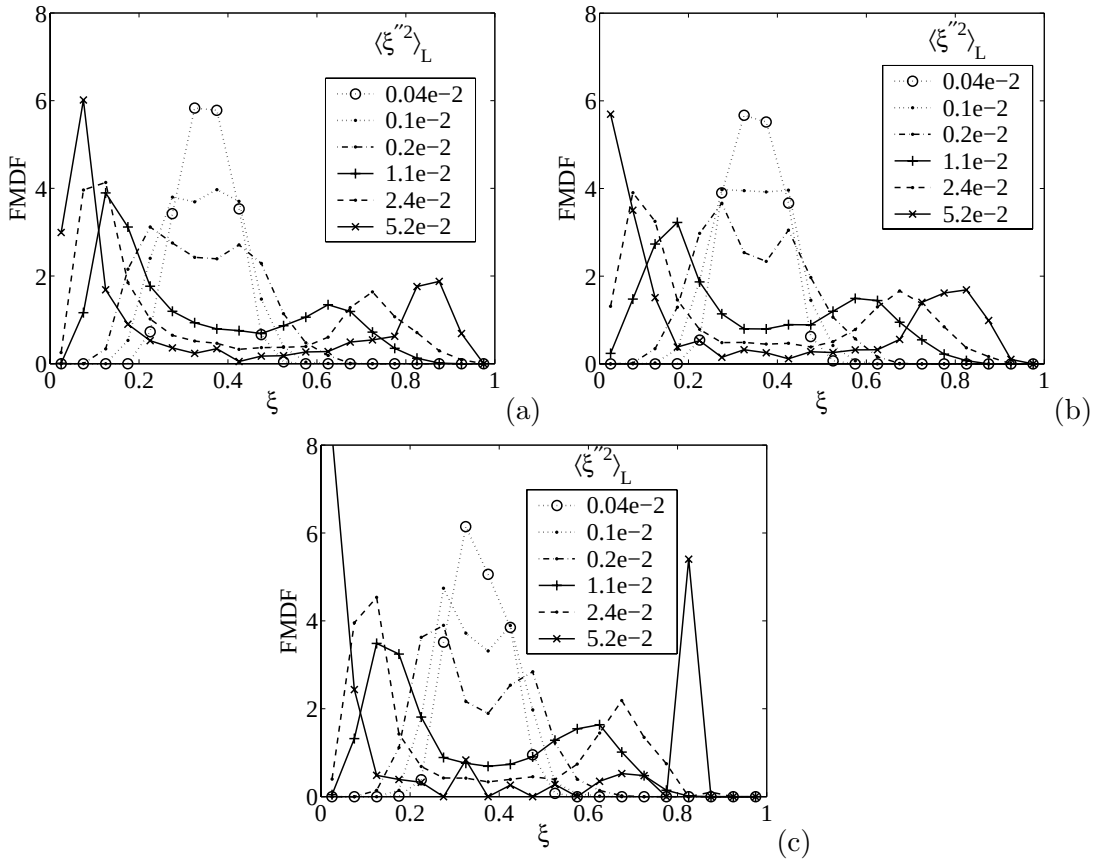


Figure 1: Conditional FMDF in flame D for $\Delta = 3.0$ mm and $\langle\xi\rangle_L = 0.35$. (a) $x/D = 7.5$; (b) $x/D = 15$; (c) $x/D = 30$.

with the left and right peak values decreasing and increasing respectively, reflecting the increase in the $\langle\xi\rangle_L$ value. This result indicates that variations of the $\langle\xi\rangle_L$ value only alter the fraction of the fuel-lean region relative to that of the fuel-rich region in the conditionally sampled SGS field.

The conditional FMDFs at different downstream locations (Fig. 1) exhibit similar characteristics to that at $x/D = 15$. The maximum value of the conditional SGS mixture fraction decreases somewhat with increasing downstream distance. Far downstream the maximum will be significantly less than unity (no pure fuel left). However, the qualitative characteristics of close-to-Gaussian and bimodal distributions are expected to remain the same, as observed in non-reacting jets[7, 10].

The filter scale is an important parameter in LES and it is important to understand how the FMDF varies with it. The results for the two filter scales (3.0 and 6.0 mm) at $x/D = 15$ (Figs. 1b & 2b) are very similar, further demonstrating that the bimodal FMDF is an inherent property of the SGS scalar with large SGS variance and that the burden on the mixing model to predict the bimodal distributions does not lessen with decreasing filter scale. The results also show that

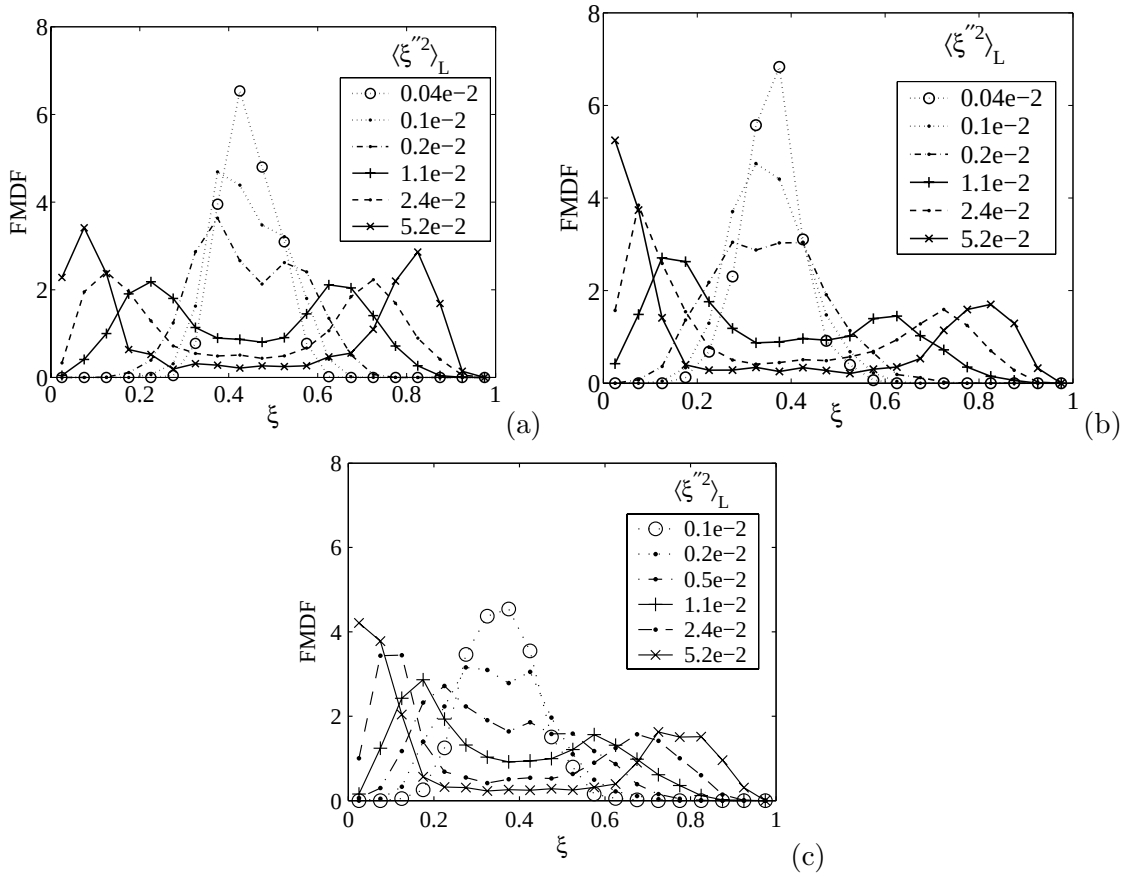


Figure 2: Conditional FMDF at $x/D = 15$. (a) flame D, $\Delta = 3.0$ mm, $\langle\xi\rangle_L = 0.45$; (b) flame D, $\Delta = 6.0$ mm, $\langle\xi\rangle_L = 0.35$; (c) flame E, $\Delta = 3.0$ mm, $\langle\xi\rangle_L = 0.35$.

the transition from unimodal to bimodal FMDF for the two filter scales (defined here as the point at which the top of the FMDF becomes flat) occurs at approximately $\langle \xi''^2 \rangle_L = 0.001$ and 0.002, respectively. This difference is related to the mean SGS variance for $\Delta = 3.0$ mm (0.0025) being smaller than that for $\Delta = 6.0$ mm (0.0034). Previous results[7, 10] have shown that in the fully developed region of a non-reacting jet the scalar FDF essentially can be collapsed by the normalized SGS variance, $\langle \xi''^2 \rangle_L / \langle \xi''^2 \rangle$, regardless of the filter size (as long as it is sufficiently large compared to the Corrsin scale). The results in Figs. 1b & 2b are qualitatively consistent with the previous results. However, in a developing flow this might not be true. Comparing Figs. 1a & 1b we find that in both cases the transition to bimodal FMDF occurs approximately at $\langle \xi''^2 \rangle_L$ =0.001, although the mean values of the SGS variance differ by nearly a factor of 2 (0.0065 vs 0.0034). These results might be because the turbulence is evolving rapidly near the nozzle.

The FMDF results show that the statistical structure of the SGS mixture fraction is qualitatively different for small and large SGS variance values. For a bimodal FMDF, the difference between the $\xi$ values for its peaks is often larger than the near-equilibrium (or mildly strained flamelets) reaction zone width in the $\xi$ space for these methane flames, $\Delta\xi_R (\approx 0.23)$, defined by the lean and rich limits that correspond to 10% of the peak CO oxidation reaction rate in laminar flames[11]. Therefore, such a mixture fraction structure is likely to limit the reaction zones in thin diffusion layers, thereby resulting in laminar flamelets. By contrast, for the well-mixed SGS mixture fraction field, the turbulence cascade is likely to dominate and the dissipation-scale scalar fluctuations largely follow the Kolmogorov-Obukhov-Corrsin predictions. Therefore, such a SGS scalar is likely to result in distributed reaction zones.

**B. The conditionally filtered scalar dissipation**

The conditionally filtered scalar dissipation, $\langle \langle \chi | \xi \rangle_\ell | \langle \xi \rangle_L, \langle \xi''^2 \rangle_L \rangle$, for the same conditions as Fig. 1 is shown in Fig. 3. Similar to the FMDF, $\langle \chi | \xi \rangle_\ell$ also has qualitatively different functional forms for small and large SGS variance. For small $\langle \xi''^2 \rangle_L$ it shows a weak dependence on $\xi$, consistent with the conditional FMDF being unimodal and not far from Gaussian, providing further evidence that the SGS mixture fraction was well-mixed. For large $\langle \xi''^2 \rangle_L$, the conditionally filtered dissipation becomes bell-shaped, with the maximum value increasing with the SGS variance value. Furthermore, the maximum value occurs at the $\xi$ value where the bimodal FMDF has the minimum, indicating that there was a sharp interface between the highly segregated SGS mixture fraction regions, which was essentially a diffusion layer (cliff) with a thickness of the order of the Corrsin scale. Because the diffusion is generally toward the scalar value at the center of the diffusion layer (cliff), independent of the chemistry, mixing models such as the interaction by exchange with the mean (IEM) model can lead to unphysical mixing across $\xi_s$ (the reaction zone).

The FMDF and the conditionally filtered dissipation results suggest that the SGS mixture

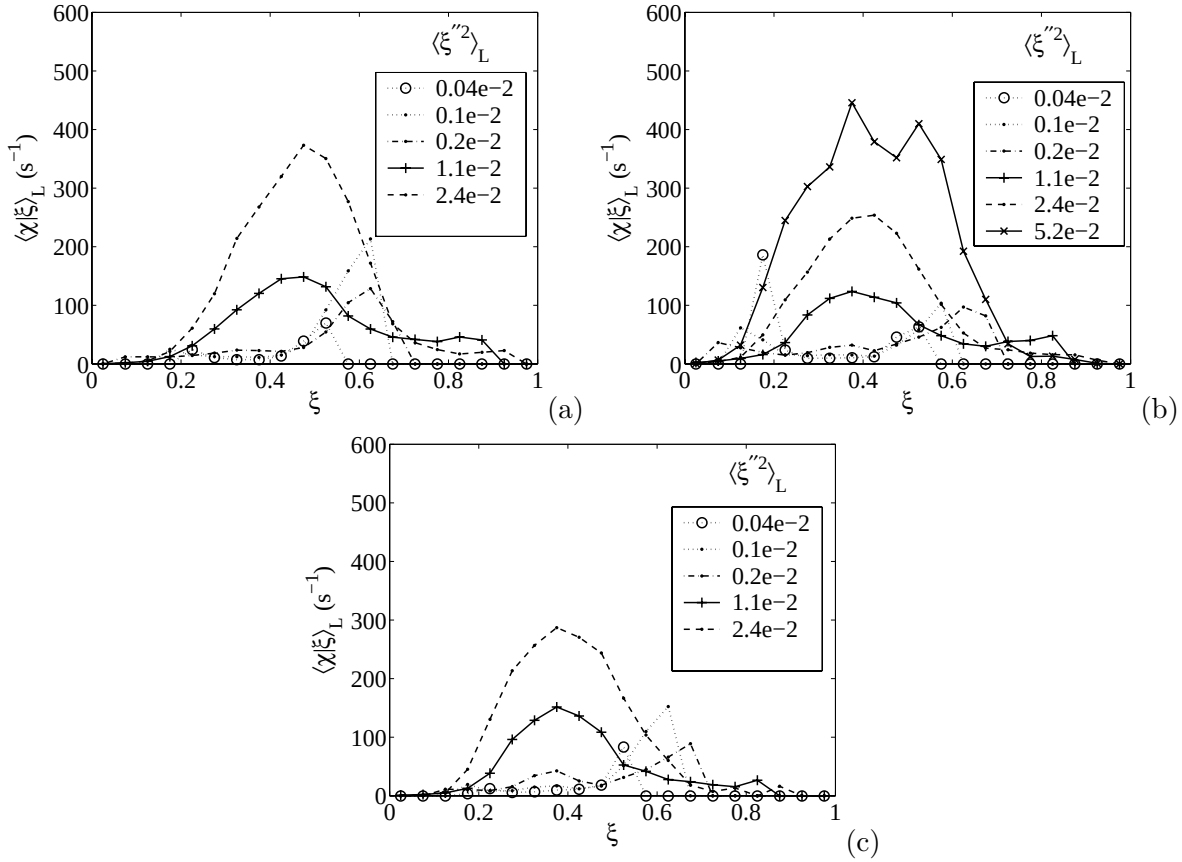


Figure 3: Conditionally filtered scalar dissipation, $\langle \langle \chi|\xi\rangle_\ell | \langle \xi \rangle_L, \langle \xi''^2 \rangle_L \rangle$, in flame D. Conditions same as in Fig. 1.

fraction structure under the condition of large SGS variance is similar to that in the counter-flow model for laminar flamelets. However, Rajagopalan and Tong[10] noted that the lean and rich mixtures in a bimodal SGS scalar generally do not have $\xi$ values of 0 and 1 respectively, a situation similar to that noted by Bish and Dahm[12]. Therefore, the laminar flamelets resulted are not simple flamelets obtained using $\xi = 0$ and 1 as boundary conditions. The FMDF results show that the boundary conditions for these flamelets are essentially the $\xi$ values for the two FMDF peaks.

The observed relationship between the scalar FMDF and conditionally filtered dissipation for small and large SGS variance is also similar to that between the scalar PDF and the conditional dissipation[7, 8]. This similarity is remarkable because while the scalar PDF and the conditional dissipation are related through the scalar PDF equation, there is no analogous equation relating the conditional FMDF and the conditionally filtered dissipation. Therefore, the relationship suggests that the dynamics of the conditional SGS fields are very similar to fully developed and rapidly evolving scalar fields, respectively. The similarities between the above results and those obtained in nonreacting flows also suggest that heat release does not change qualitatively the structure of

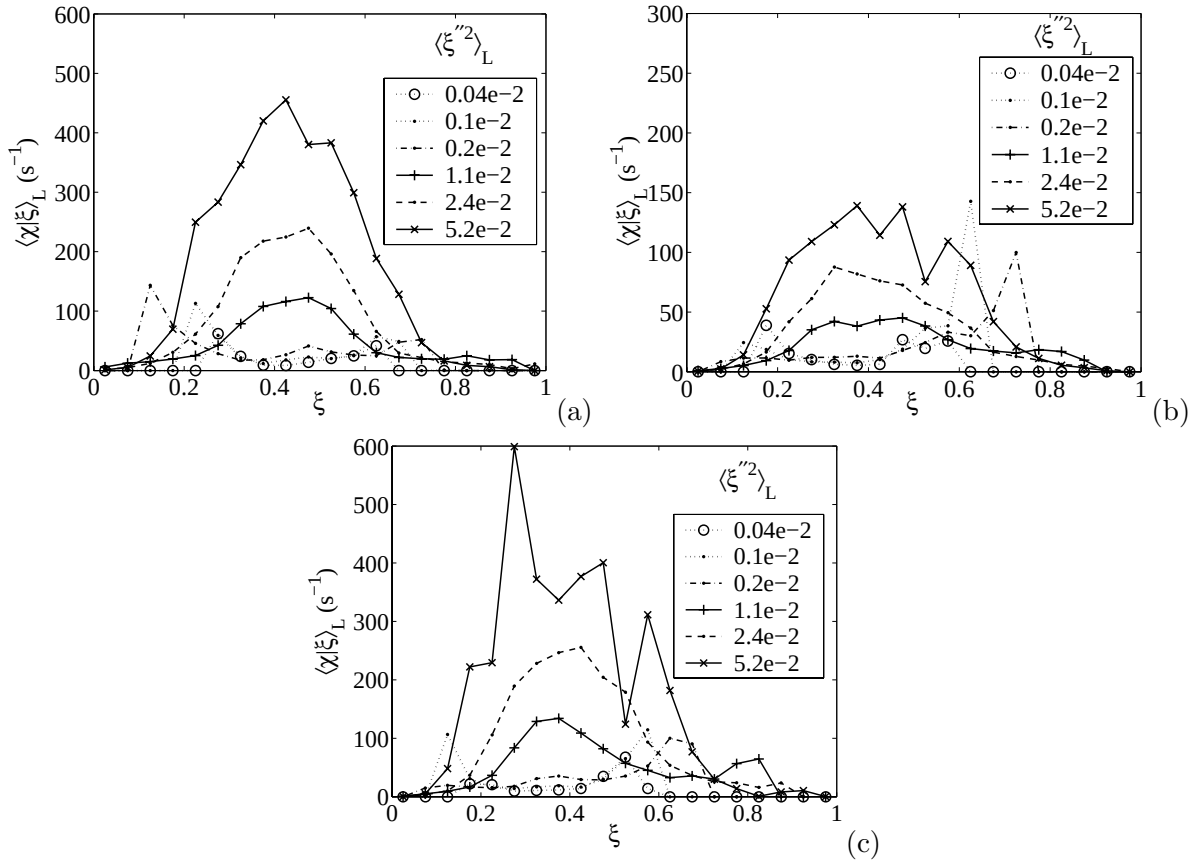


Figure 4: Conditionally filtered scalar dissipation, $\langle \langle \chi|\xi \rangle_\ell | \langle \xi \rangle_L, \langle \xi''^2 \rangle_L \rangle$. Conditions same as in Fig. 2.

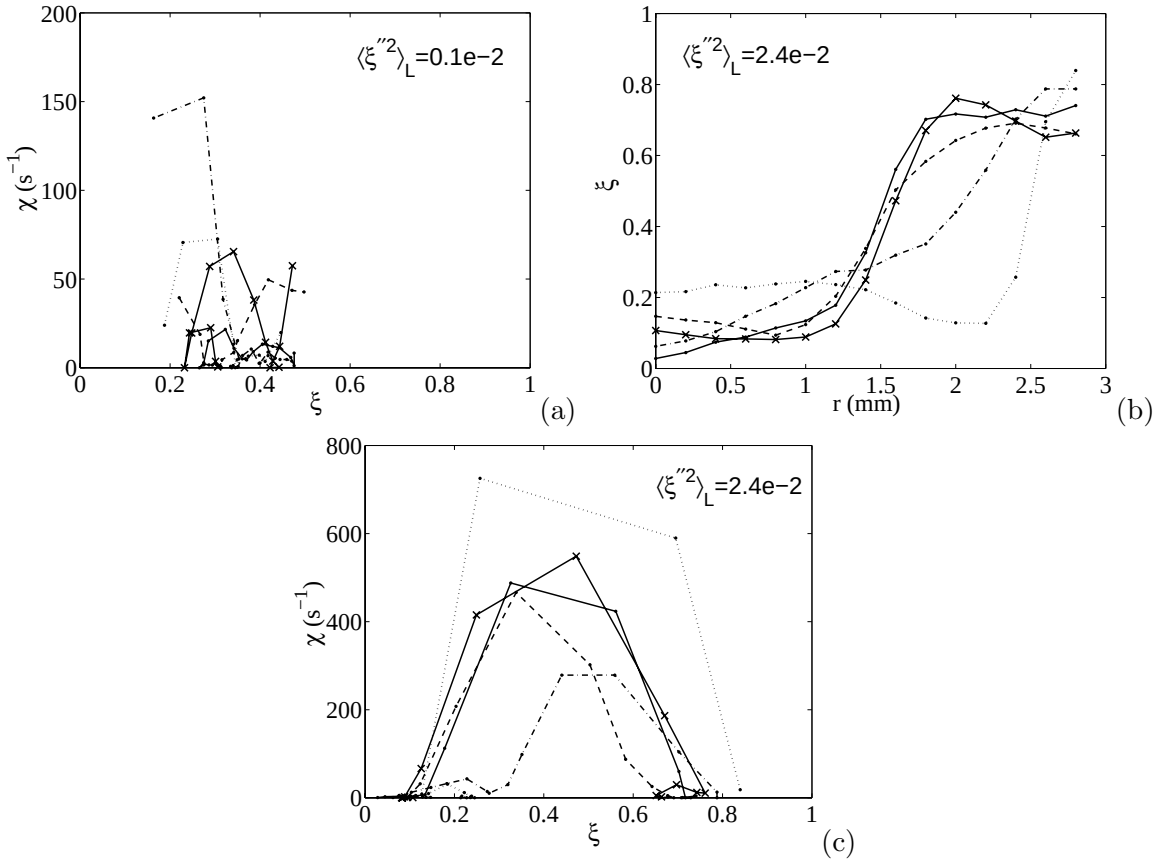


Figure 5: Conditional profiles in flame D for $\langle\xi\rangle_L = 0.35$. $x/D = 15$, $\Delta = 3.0$ mm. (a) and (c) $\chi - \xi$; (b) $\xi$.

the SGS mixture fraction fields, although other aspects of the SGS scalar may still be influenced by heat release.

The conditionally filtered dissipation at $x/D = 15$ for the larger filter scale $\Delta = 6.0$ mm in Fig. 4b has similar characteristics to those for $\Delta = 3.0$ mm, but the maximum value is much lower for the same large SGS variance value. For example, for $\langle\xi''^2\rangle_L = 0.052$, the maximum value of $\langle\chi|\xi\rangle_\ell$ is above 400 s$^{-1}$ for $\Delta = 3.0$ mm while it is only near 150 s$^{-1}$ for $\Delta = 6.0$ mm. We argue that this difference is due to two factors. First, the transition from unimodal to bimodal FMDF occurs at a smaller SGS variance value for $\Delta = 3.0$ mm (Figs. 1b and 2b). Therefore, we expect that for a given SGS variance, the bimodality is stronger, and therefore the dissipation is higher. Second, because of the relatively low Reynolds number of the flame, the filter sizes employed are not very large compared to the scalar dissipation scales ($\approx 0.5$ mm in cliffs). Consequently, for the same SGS variance value, the average width of the diffusion layer sampled must be smaller in when the filter size decreases, resulting in a higher in-layer dissipation rate.

The conditionally filtered dissipation for $\langle\xi\rangle_L$ =0.45 (Fig. 4a) has similar functional forms to those for $\langle\xi\rangle_L = 0.35$, in contrast with the larger changes in the FMDF, especially for large SGS variance values. Because the peak region of the conditionally filtered dissipation is dominated by the cliffs, its weaker dependence on $\langle\xi\rangle_L$ indicates that essentially the same cliffs were captured by the conditional sampling procedure. The ramps were sampled differently (see Fig. 2a for FMDF), but they correspond to much lower dissipation values, and therefore do not affect the overall functional form of $\langle\chi|\xi\rangle_\ell$.

Comparisons among the results for the conditionally filtered dissipation at the three downstream locations (Fig. 3) show that the maximum value for $\langle\chi|\xi\rangle_\ell$ with large SGS variance decreases from $x/D = 7.5$ to 15, which is due to two reasons. First, the dissipation length scale generally increases with the downstream distance, resulting in a larger diffusion layer thickness and a smaller $\langle\chi|\xi\rangle_\ell$. Second, for large SGS variance there are extinction events at $x/D = 15$ compared to nearly no extinction at $x/D = 7.5$[13], thereby reducing the scalar diffusivity, and consequently the conditionally filtered dissipation. From $x/D = 15$ to 30 the dissipation length scale further increases, which tends to reduce the $\langle\chi|\xi\rangle_\ell$. However, most extinguished fluid parcels had reignited at this location. Therefore, $\langle\chi|\xi\rangle_\ell$ tends to increase. Due to these competing effects, the maximum value for the conditional $\langle\chi|\xi\rangle_\ell$ at $x/D = 30$ increases slightly compared to that at $x/D = 15$.

The results for the conditional FMDF (Fig. 2c) and $\langle\chi|\xi\rangle_\ell$ (Fig. 4c) for flame E are similar to those for flame D. The jet velocity is higher in flame E, resulting in higher strain rates and more local extinction events. The higher strain rates tend to result in higher scalar dissipation rates. In addition, local extinction may lead to stronger entrainment since heat release tends to suppress entrainment[14], thereby enhancing the dissipation in cliffs. However, local extinction also tends to reduce the diffusivity and dissipation. Moreover, the higher Reynolds number and possibly the local extinction reduced the local scalar dissipation length scale, potentially resulting in insufficient measurement resolution and lower measured dissipation rate. Probably as a result of these competing effects, the maximum value for $\langle\chi|\xi\rangle_\ell$ for flame E (Fig. 4E) is approximately equal to (or slightly smaller than) that for flame D. Further understanding of the effects may require measurements of flame E at a higher resolution.

The above results indicate that the SGS mixture fraction fields have different spatial structures for small and large SGS variance values. We provide in Fig. 5 several examples of conditional SGS mixture fraction and mixture fraction-scalar dissipation profiles. For small SGS variance, the $\chi - \xi$ profiles have no clear structures, consistent with the well-mixed SGS mixture fraction. The rms (the instantaneous standard deviation) and dissipation-scale SGS mixture fraction fluctuations are smaller than the reaction zone width $\Delta\xi_R$ ($\approx 0.23$). The measured scalar dissipation values (even after multiplying them by a factor of three using the assumption of local isotropy) are smaller than

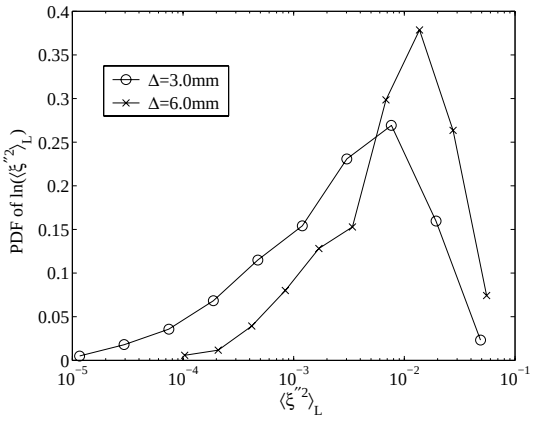


Figure 6: PDF of $ln(\langle\xi''^2\rangle_L)$ in flame D at $x/D = 15$. $\langle\xi\rangle_L = 0.35$.

the extinction dissipation rate for a steady laminar flame ($\chi_q = 400\ s^{-1}$ for the fuel considered), indicating that the conditional SGS flame was in the form of quasi-equilibrium distributed reaction zones. For large SGS variance, the SGS $\xi$ profiles show large jumps in mixture fraction (the cliff), effectively limiting the reaction zone to within the structure and resulting in laminar flamelets. The $\chi - \xi$ profiles are also consistent with this structure. For several profiles the dissipation (even one component) exceeds the extinction value. Therefore, the local extinction events were most likely in the form of flamelet extinction.

The results also suggest that at a given location in a turbulent flame, the SGS reaction zones fluctuate between distributed reaction zones and laminar flamelets due to the occurrences of the well mixed and highly nonpremixed SGS mixture fraction fields. This cause for the occurrences of both flame structures is different from previous arguments based on the fluctuations in the scalar dissipation rate due to the turbulence cascade. The scalar dissipation rate at a point, by itself, does not provide sufficient information about the structure of the local mixture fraction field. The variations of the flame structure with the SGS mixture fraction structure suggest that mixing models need to be able to capture the well-mixed and bimodal distributions to account for these flame structures.

To further understand the impact of the SGS mixture fraction structure on the flame structure, it is important to quantify the potential contributions to the heat release from each type of flame structure. We first quantified the portion of the SGS fields containing ramp-cliff structures by plotting the PDF of $ln\langle\xi''^2\rangle_L$ in flame D at $x/D = 15$ (Fig. 6). The PDFs are approximately log-normally distributed with the peaks located at about $\langle\xi''^2\rangle_L = 0.0067$ and 0.014, respectively. The conditional FMDF (Fig. 1b) is already bimodal for the $\langle\xi''^2\rangle_L$ values at the peak location

Table 1: Contributions to the scalar dissipation rate from the ramp-cliff structure ($\langle\xi''^2\rangle_L > V$) within the reaction zone for different $V$ values.

| flame | $\Delta$ | $V = 0.001$ | 0.002 | 0.005 | 0.011 | 0.024 |
|---|---|---|---|---|---|---|
| D | 3.0mm | 0.879 | 0.739 | 0.527 | 0.254 | 0.049 |
| D | 6.0mm | 0.981 | 0.934 | 0.815 | 0.532 | 0.189 |
| E | 3.0mm | 0.851 | 0.69 | 0.451 | 0.182 | 0.026 |
| E | 6.0mm | 0.97 | 0.901 | 0.731 | 0.41 | 0.102 |

of the $ln\langle\xi''^2\rangle)_L$ PDF, indicating that well over 30% of the SGS scalar field contained ramp-cliff structures ($\langle\xi''^2\rangle_L > 0.005$ and 0.01 for $\Delta = 3$ and 6 mm, respectively). These results are essentially independent of the chemistry. Among these SGS fields, only those containing scalar value jumps larger than $\Delta\xi_R$ could result in laminar flamelets.

To quantify the potential contributions to the heat release from the bimodal SGS fields, which is chemistry (reaction zone width) dependent, we calculated the ratio of the contributions to the scalar dissipation rate from the portion of the ramp-cliff structure where the reaction zone resides ($\xi_s - \frac{\Delta\xi_R}{2} < \xi < \xi_s + \frac{\Delta\xi_R}{2}$) to those from all the reaction zones as ,

$$\frac{\langle\chi|\xi_s - \frac{\Delta\xi_R}{2} < \xi < \xi_s + \frac{\Delta\xi_R}{2}, \langle\xi''^2\rangle_L > V\rangle}{\langle\chi|\xi_s - \frac{\Delta\xi_R}{2} < \xi < \xi_s + \frac{\Delta\xi_R}{2}\rangle} Prob\{\langle\xi''^2\rangle_L > V|\xi_s - \frac{\Delta\xi_R}{2} < \xi < \xi_s + \frac{\Delta\xi_R}{2}\}, \qquad (7)$$

because heat release is, to the first order approximation, proportional to the scalar dissipation rate. The results for several $V$ values are given in Tab. 1. For both filter scales the scalar dissipation for large SGS variance ($\langle\xi''^2\rangle_L > 0.005$ and 0.01, respectively) accounts for more than 50% of the total scalar dissipation within the reaction zones, suggesting that a significant amount of the heat release came from the ramp-cliff structure, although it only occupied a small fraction of the spatial volume. These results indicate that bimodal SGS mixture fraction associated with the ramp-cliff structure and the resulting laminar flamelets play important roles in nonpremixed/partially premixed flames and must be properly accounted for by mixing models.

### C. The conditional mixture fraction-temperature FMDF

The conditional mixture fraction-temperature FMDF, $\langle F_{\xi T}|\langle\xi\rangle_L, \langle\xi''^2\rangle_L\rangle$, for flame D and E at $x/D = 7.5$ is shown in Fig. 7. The filtered mixture fraction, $\langle\xi\rangle_L$, was again set to the stoichiometric

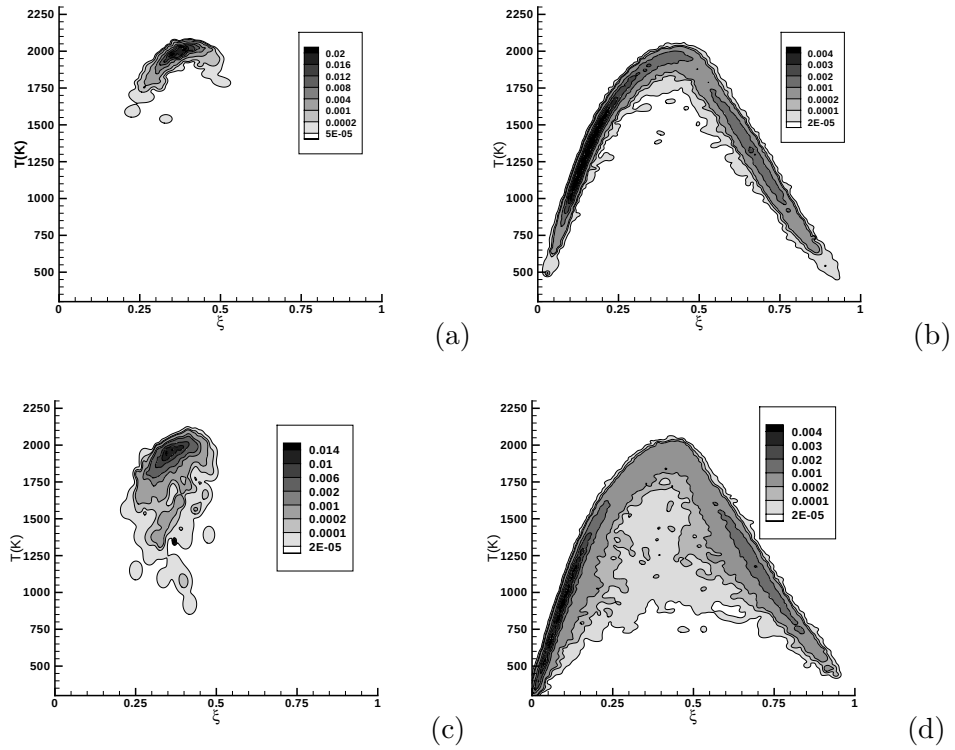


Figure 7: Conditional FMDF at x/D=7.5. (a) flame D, $\langle \xi''^2 \rangle_L$=0.0013; (b) flame D, $\langle \xi''^2 \rangle_L$=0.066; (c) flame E, $\langle \xi''^2 \rangle_L$=0.0011; (d) flame E, $\langle \xi''^2 \rangle_L$=0.081.

mixture fraction, $\xi_s (= 0.35)$, to maximize the probability of the SGS field containing reaction zones. For flame D there was little local extinction at this location and the FMDF for both small and large SGS variance is concentrated not far from the equilibrium values. For small SGS variance, e.g. $\langle \xi''^2 \rangle_L \approx 0.0047$ (Fig 1a), the conditional FMDF is unimodal. The peak of the FMDF (most samples) is near the equilibrium values. Due to the well mixed SGS scalar the SGS reactions are expected to be in the quasi-equilibrium reaction zones regime. For flame E there was some local extinction as reflected by the low temperature but the results are otherwise similar to those for flame D.

As the SGS variance increases, the FMDF becomes bimodal (Figs. 7b & d) with the bimodality stronger for larger SGS variance. The peaks are at $\xi = 0.17$ and 0.62, indicating that the rich and lean mixtures in the SGS field (i.e., a grid cell) were essentially segregated. Furthermore, there was a sharp interface (diffusion-layer) separating the two regions, across which there was a large scalar value jump (also see the discussion on the conditionally filtered scalar dissipation rate below). For flame D although most samples were still far from extinction, the temperature near $\xi = 0.4$ was already lower than that for the small SGS variance. For a bimodal FMDF the SGS scalar contains two relatively well-mixed mixtures corresponding to the two peaks of the

FMDF. The difference between the $\xi$ values of the two mixtures is often greater than the reaction zone width in the $\xi$ space for these methane flames, $\Delta\xi_R(\approx 0.23)$, defined by the lean and rich limits that correspond to 10% of the peak CO oxidation reaction rate in mildly strained laminar flames[11]. Therefore, such a mixture fraction structure limits the reaction zones in thin diffusion layers, thereby resulting in laminar flamelets. By contrast, for the well-mixed SGS mixture fraction field, the turbulence cascade is likely to dominate and the dissipation-scale scalar fluctuations largely follow the Kolmogorov-Obukhov-Corrsin predictions. Therefore, such a SGS scalar is likely to result in distributed reaction zones. For flame E the FMDF values near equilibrium are lower than for flame D and there was a relatively large probability of local extinction due to the large scalar dissipation rate with temperature as low as 1000K. These results are consistent with the mixture fraction FMDF[15]

At $x/D = 15$, there were more extinguished samples for both flame D and E (not shown). For small SGS variance, the FMDF shape is similar to that at $x/D = 7.5$. For large SGS variance, the FMDF peak on the rich side is broader due to the increased temperature variations, therefore the peak value is lower. The amount of local extinction in flame E (not shown) was approximately 5 times that in flame D. At $x/D = 30$, the probability of local extinction was approximately 2-3 times lower than at $x/D = 15$ because the scalar dissipation was reduced as the flames evolved downstream.

The filter scale is an important parameter in LES and it is important to understand how the FMDF varies with it. Our previous results have shown that increasing the filter scale does not alter the shape of the FMDF. The results in the present study (not shown) are consistent with this finding.

### D. The conditionally filtered scalar dissipation conditional on both the mixture fraction and temperature

The conditionally filtered scalar dissipation, $\langle\langle\chi|\xi,T\rangle_\ell|\langle\xi\rangle_L,\langle\xi''^2\rangle_L\rangle$, for the same conditions as Fig. 7 is shown in Fig. 8. Here we have limited the domains of the conditioning variables $\xi$ and $T$ to those of the corresponding FMDF shown in Fig. 7. Similar to the FMDF, $\langle\chi|\xi,T\rangle_\ell$ also has qualitatively different functional forms for small and large SGS variance. At $x/D = 7.5$, flame D (Figs. 8a&b) had little local extinction. For small $\langle\xi''^2\rangle_L$ the dissipation has a relatively weak dependence on $\xi$, consistent with the conditional FMDF being unimodal. However, a higher dissipation rate generally corresponds to a lower temperature. The observed temperature-scalar-dissipation correlation for a fixed mixture fraction is consistent with the expectation that in quasi-equilibrium distributed reaction zones the temperature decreases as the scalar dissipation increases[16].

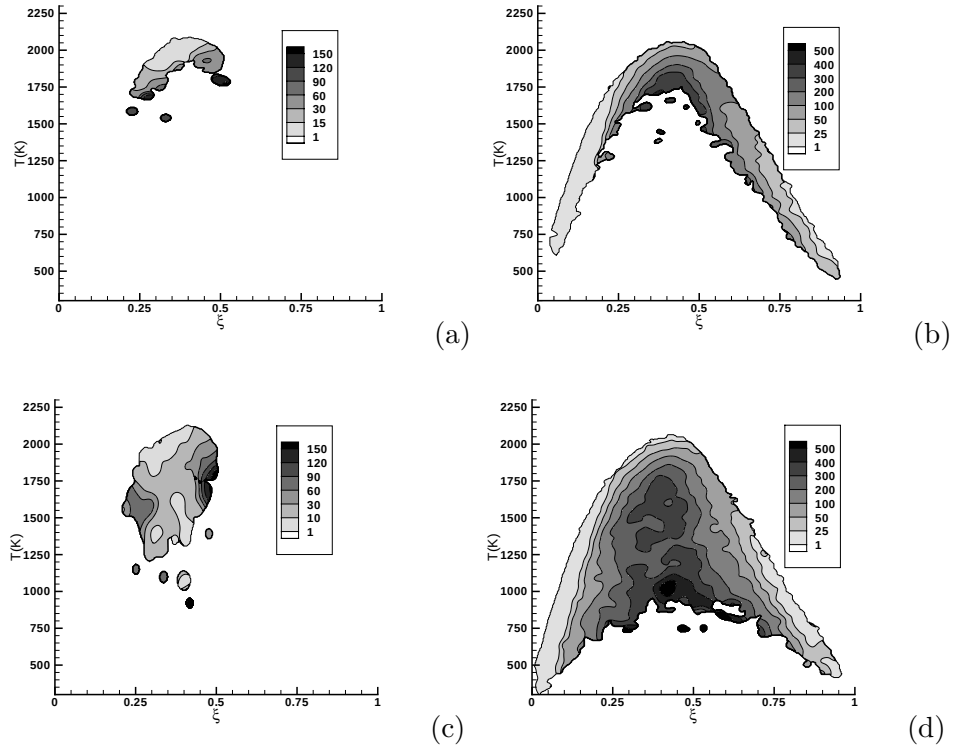


Figure 8: Conditionally filtered mixture fraction dissipation. Conditions same as in Fig. 7.

In flame E the dissipation for the samples close to equilibrium has a similar dependence on $\xi$ and T (Fig. 8c). However, flame E already had a significant amount of local extinction but the scalar dissipation near the stoichiometric mixture fraction at lower temperature (1250-1750K) does not depend strongly on temperature.

For large $\langle \xi''^2 \rangle_L$ , the conditionally filtered dissipation in flame D (Fig. 8b) is generally large near $\xi = 0.4$ to 0.45, where the maximum gradient in the ramp-cliff structure was located[15]. The maximum value increases with the SGS variance value (not shown). Near the equilibrium values the scalar dissipation is generally larger for lower temperature, consistent with the characteristics of strained laminar flamelets. Again, at $x/D = 7.5$, flame D had little local extinction; therefore the conditional dissipation does not extend to very low temperatures. For flame E, the samples close to equilibrium are similar to those in flame D. Further away from equilibrium at lower temperatures the dissipation rate was larger and there was a significant amount of local extinction. The highest value (one component) of approximately $700s^{-1}$ observed in some images (not shown), which well exceeded the extinction dissipation rate for a steady laminar flamelets, occurred at very low temperature (approximately 750K). Considering the reduced diffusivity at these temperatures, the high dissipation rate was likely caused by very high strain rates. Because the SGS scalar contained ramp-cliff structure, these samples were most likely extinguished laminar flamelets.

At $x/D = 15$ flame D (not shown) had a larger number of extinguished samples with very low temperatures ($< 1300K$) and the dissipation is qualitatively similar to those for flame E at $x/D = 7.5$. When the SGS variance is small, the dissipation rate increases with decreasing temperature for the burning samples. The dependence is insensitive to the $\xi$ values, similar to the results shown in Fig. 2c. For the extinguished samples the peak conditional dissipation rate is approximately $150s^{-1}$, below the extinction rate for steady laminar flamelets ($\approx 400s^{-1}$)[14]. Therefore, these samples might have been extinguished upstream. As they were advected downstream to the measurement location the scalar dissipation rate had reduced but they had not yet mixed with high temperature parcels to reignite. Therefore, their temperatures remained low. The results for flame E show a similar trend (not shown). Previous DNS of nonpremixed combustion in isotropic turbulence[17] also showed a similar evolution process.

For large SGS variance both flame D and E (nor shown) had extinguished samples, with the latter having approximately 5 times more but the scalar dissipation results are similar to those at $x/D = 7.5$. The maximum conditionally filtered dissipation rate is reduced to $500s^{-1}$ for both flames.

At $x/D = 30$ (not shown), there was a significant amount of reignition and the probability for extinguished samples was reduced. For small SGS variance, the dependence of the dissipation on $\xi$ is weaker compared to $x/D = 7.5$ and 15. For large SGS variance the maximum conditionally filtered dissipation rate remains at approximately $500s^{-1}$ for both flames. However, the probability of occurrence for the large variance is smaller compared to the upstream locations, consistent with the reignition and the reduced degree of local extinction.

**E. The conditionally filtered temperature dissipation**

The above results indicate that the different structures of the SGS mixture fraction fields for small and large SGS variances result in different conditionally filtered scalar dissipation. Through interaction with combustion chemistry, the SGS mixture fraction fields will result in qualitatively different temperature dissipation structure. We now examine the conditionally filtered temperature dissipation, which is shown in Fig. 9. In flame D at $x/D = 7.5$ the temperature is close to the equilibrium values for small SGS variance. Near $\xi = 0.45$ the flame reaches the local maximum temperature, leading to the lowest temperature dissipation. Away from $\xi = 0.45$ the temperature dissipation is small near the equilibrium values and increases with decreasing temperature. There is some similarities between the conditional temperature dissipation and the conditional scalar dissipation samples for the rich and lean mixtures because for these mixtures there exists a correlation between $\xi$ and $T$ near the equilibrium curve (positive for $\xi < 0.4$ and negative for $\xi > 0.4$). Therefore, the temperature dissipation increased with the scalar dissipation for these mixture fraction values. In flame E there were some non-burning samples with higher $\chi_T$ but the

results are otherwise similar to those for flame D.

For large SGS variance, flame D was still close to fully burning. For the samples not far from equilibrium, large temperature dissipation values occurred in rich mixtures with $\xi$ values ranging from 0.5 to 0.65, but not in the lean mixtures. This phenomenon is a result of the strained laminar flamelet structure. For a flamelet far from extinction $T = T(\xi, \chi_s)$ and $\frac{\partial T}{\partial y} = \frac{\partial T}{\partial \xi}\frac{\partial \xi}{\partial y}$, where $\chi_s$ is the scalar dissipation rate at the stoichiometric mixture fraction. Because $\frac{\partial T}{\partial \xi}$ is V-shaped with a minimum (zero) near $\xi = 0.45$ and at the same time $\frac{\partial \xi}{\partial y}$ is bell-shaped with its peak value located near $\xi = 0.5$ (Fig. 8d), large values of $\frac{\partial T}{\partial \xi}\frac{\partial \xi}{\partial y}$ and the temperature dissipation occur for $\xi$ values ranging from 0.5 to 0.65. Further away from equilibrium, there are some large $\chi_T$ values on both the rich and lean side of the flame. An examination of the line images (not shown) indicated that the lean sides of the images have the shape of strained laminar flamelets, indicating that the lean sides of the laminar flamelets were nearly fully burning. However, the large $\chi_T$ values on the rich sides come from images containing straight lines in the $\xi - T$ space, running from $\xi_s$ to the rich side, indicating that the samples were being mixed but not burning. At this location a significant portion of the SGS stoichiometric mixture for large SGS variance might be the pilot flame gas, suggesting that the high temperature dissipation values are largely due to the mixing of the pilot gas with the rich mixtures. Because the scalar dissipation rate was high, mixing was much faster than reaction, resulting a mixing line (mixing without reaction). Similar straight mixing lines have been observed in double scalar mixing layers[18]. This observation suggests that each of these laminar flamelets was split by the pilot gas, effectively forming two flamelets, one lean and one rich. It has been suggested [5, 19] that the pilot gas had been throughly mixed at $x/D = 7.5$. While on average the amount of pilot gas may be small at this location, the conditional samples for large SGS variance still contained a significant amount of pilot gas because these conditional samples were much less well mixed. In fact nearly pure pilot gas was found as far as $x/D = 15$ (see the discussions below).

The results for the near equilibrium samples in flame E are similar except that the largest $\chi_T$ comes from the mixing of the pilot and the lean mixtures. For the extinguished samples at much lower temperature ($< 1200K$) the line images in the $\xi - T$ space include ones running from near stoichiometric mixture to both sides as well as straight lines running from the lean side to the rich side of the equilibrium curve, consistent with extinguished laminar flamelets.

At $x/D = 15$ a number of extinction events occurred for both small and large SGS variance values. In flame D for small SGS variance the samples close to equilibrium had similar temperature dissipation structures to those at $x/D = 7.5$ with low $\chi_T$ near $\xi = 0.45$ (Fig. 3e). The extinguished samples with very low temperatures ($< 1300K$) generally had small temperature dissipation because the temperature gradient was reduced by mixing. In addition, lower diffusivity resulted from the reduced temperature could also contribute to the lower dissipation rates. The samples with

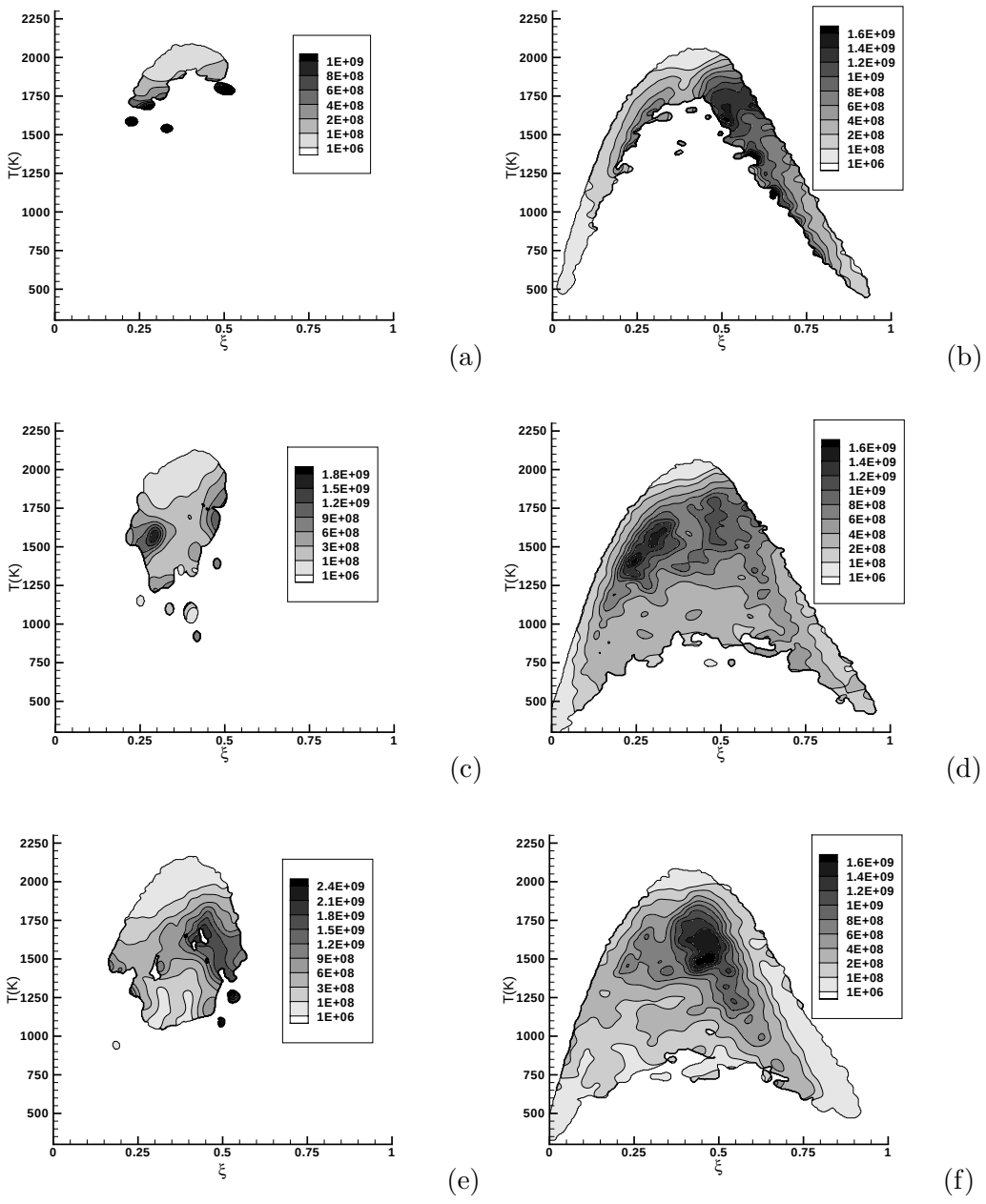


Figure 9: Conditionally filtered temperature dissipation. (a)-(d) conditions same as in Fig. 7. (e) flame D, x/D=15, $\langle \xi''^2 \rangle_L$=0.0030, (f) flame D, x/D=15, $\langle \xi''^2 \rangle_L$=0.069.

intermediate temperatures (1300-1600K) had the highest temperature dissipation, likely a result of mixing between the burning and extinguished samples. The dependence on the mixture fraction is relatively weak compared to samples with higher temperature because T and $\xi$ no longer follow the equilibrium relationship. Therefore, these samples had high $\chi_T$ but relatively low $\chi$.

For large SGS variance, $\chi_T$ for the burning samples (close to equilibrium) is similar to that at $x/D = 7.5$ with large values near $\xi = 0.55$. The dissipation is maximum near $\xi = 0.5$ and $T = 1600K$. The line images going through this region in the $\xi - T$ space (not shown) indicate that the lean sides of the images mostly have the shape of strained laminar flamelets. There are a few straight lines, suggesting more intense mixing between the pilot and the air than at x/D=7.5, probably due to the spreading of the turbulence towards the lean side. The rich sides contain more straight lines in the $\xi - T$ space than at x/D=7.5, running from $\xi_s$ to the rich sides, again indicating that these samples were being mixed but not burning. At this location we expect that the proportion of pilot gas at the stoichiometric mixture to be much smaller compared to $x/D = 7.5$, but apparently there was still a sufficient amount to form a mixing line on the rich side. Therefore, the high temperature dissipation is largely due to the rapid mixing of the pilot gas with the rich mixtures. The mixing was faster than the reactions, resulting a mixing line. Again, the results suggest that each of these laminar flamelet was split by the pilot gas to form two flamelets with one on the lean side burning and the one on the rich side extinguished. For the samples at much lower temperature ($< 1200K$) the line images in the $\xi - T$ space are straight lines from the lean to the rich side, consistent with extinguished laminar flamelets. There is no apparent evidence of the pilot separating the lean and rich side, probably because the pilot gas was already mixed with the rest of the fluid due to the large $\chi$ values in these flamelets. The results for flame E (not shown) are similar.

At $x/D = 30$ (not shown) for small SGS variance $\chi_T$ is low for high temperatures and is higher for intermediate temperatures (1500-1800K). Due to reignition there were fewer samples with temperature below 1500K. For large SGS variance (not shown), $\chi_T$ has two peaks near $\xi = 0.3$ and 0.5 and $T = 1600K$ although the peak values are smaller. These results are again due to mixing of near stoichiometric mixture with lean and rich mixtures. The dissipation rate is approximately the same for both peaks whereas at $x/D = 7.5$ and 15 one peak dominates.

The temperature dissipation results indicate that for small SGS variance, which corresponds to distributed reaction zones, there was temperature mixing in the absence of significant mixture fraction mixing. On the other hand, for large SGS variance, mixture fraction mixing and temperature mixing proceeded simultaneously as in laminar flamelets. These qualitatively different properties of SGS mixing must be reflected by mixing models.

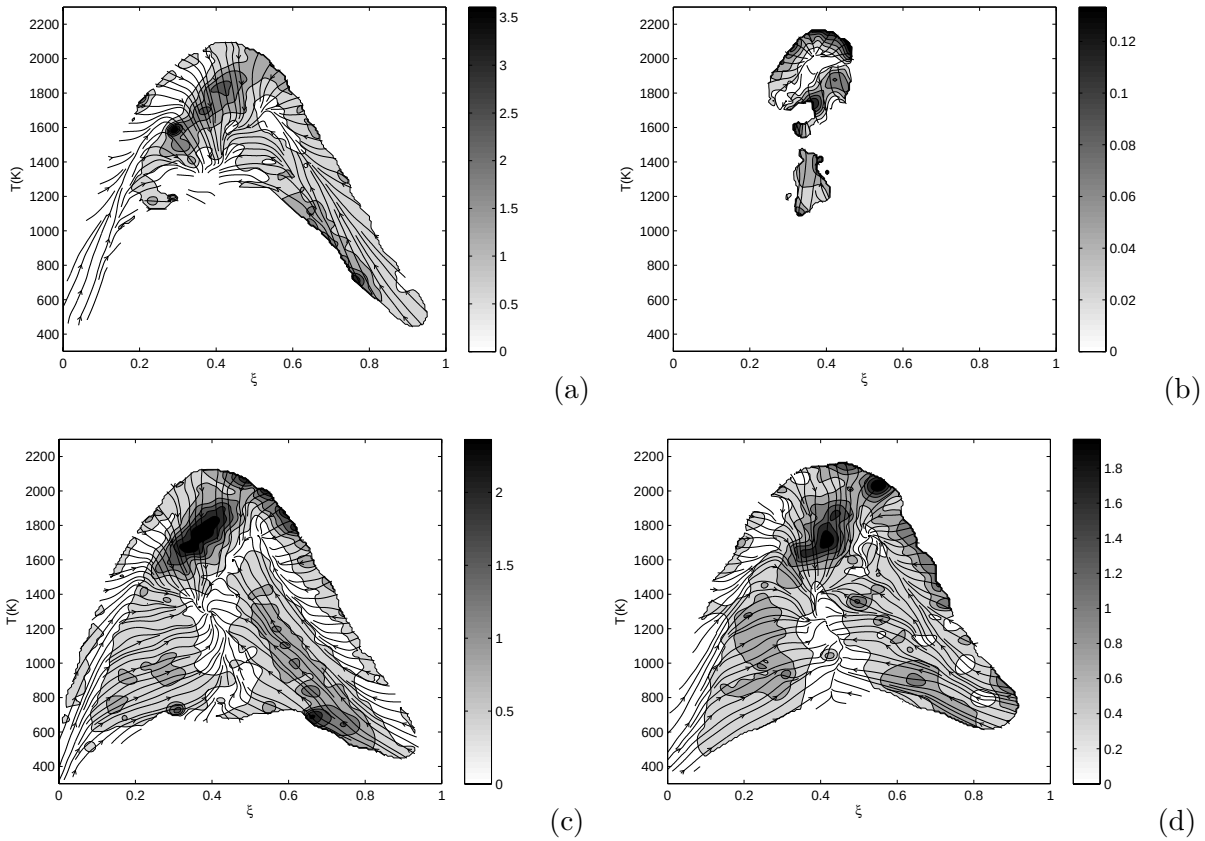


Figure 10: The mean conditionally filtered scalar diffusion and temperature diffusion conditional on both the mixture fraction and temperature for $\Delta = 3.0mm$ and $\langle\xi\rangle_L = \xi_s$ at $x/D = 15$ in flame D. The two diffusion terms are given as streamlines with the magnitude of the diffusion velocity in the $\xi - T$ space in grayscales. (a) $x/D = 7.5$ and $\langle\xi''^2\rangle_L = 0.024$; (b) $x/D = 15$ and $\langle\xi''^2\rangle_L = 0.001$ and (c) $x/D = 15$ and $\langle\xi''^2\rangle_L = 0.024$; (d) $x/D = 30$ and $\langle\xi''^2\rangle_L = 0.024$.

### F. Conditionally filtered mixture fraction and temperature diffusion

The conditionally filtered scalar and temperature diffusion conditional on both the mixture fraction and temperature are shown in Fig. 10. The two diffusion terms can be regarded as a diffusion velocity of the FJDF in the $\xi - T$ space and are represented as streamlines. For Flame D at $x/D = 7.5$ (not shown but similar to the results in Fig. 10b) the streamlines starting from the equilibrium curve near the stoichiometric mixture fraction generally move towards a stagnation point at $\xi \approx 0.4$ and $T = 1300K$. This point appears to be the "center" of diffusion, but does not necessarily corresponds to the conditional mean mixture fraction and temperature. For large SGS variance (Fig. 10a) the streamlines for very rich and lean mixtures generally move along the direction of the equilibrium curve, which may be due to the pilot flame separating the rich and lean mixtures. These streamlines are essentially a result of mixing between the pilot and the fuel/air streams without much reactions. They turn near $\xi \approx 0.27$ and $T = 1600K$ and near $\xi \approx 0.55$

and $T = 1600K$ towards the stagnation point. The temperature dissipation rate is large near the turning point.

At $x/D = 15$ the results for small SGS variance (Fig. 10b) are similar to those at $x/D = 7.5$ except that there were more local extinction events and there are more streamlines originating from low temperature regions ($\sim 1000K$). For large SGS variance (Fig. 10c) there appears to be less influence of the pilot compared to the results at $x/D = 7.5$ . For the lean mixtures the streamlines turn towards the stagnation point as early as $\xi \approx 0.15$ and $T = 1300K$. There were more low temperature samples away from the equilibrium. For these samples the streamlines move primarily in the direction of mixture fraction towards $\xi \approx 0.4$ with only modest increases in temperature. Near $\xi = 0.4$ they move largely in the direction of $T$. These trends suggest that for these samples the mixture fraction diffusion was initially much faster than the temperature diffusion. For rich samples the influence of the pilot is still evident with the streamlines turning near $\xi \approx 0.5$ and $T = 1600K$ towards the stagnation point. However, near the equilibrium curve the streamlines are not in the direction of this curve, but are nearly in the direction of $\xi$, suggesting that there were more low temperature samples towards which the near equilibrium samples diffuse. In the low temperature region the temperature diffusion was faster than for the lean samples.

At $x/D = 30$ the results for small SGS variance are similar to those at $x/D = 15$. For large SGS variance (Fig. 10d) the influence of the pilot is much less evident for both very lean and rich samples with the streamlines moving toward $\xi \approx 0.4$, indicating that the SGS mixing had progressed much further and there was little pure pilot gas left.

### G. Noise correction and resolution estimation for scalar dissipation rate measurements in turbulent partially premixed flames

In turbulent combustion research much effort has been devoted to measurements of the scalar dissipation rate. Because the scalar dissipation rate in a turbulent flame comes primarily from the smallest scalar length scales, its measurements require high spatial resolution. At the same time, the scalar fluctuations at these scales are generally much smaller than the energy-containing fluctuations, requiring low measurement noise to achieve an adequate signal-to-noise ratio for dissipation rate measurements. In practice, however, none of the two requirements are guaranteed. Often, the resolution of the measurement system is comparable to the smallest length scales and the noise contribution to the dissipation rate is significant, potentially resulting in significant errors in the measured dissipation rate.

In the present work we developed a local analysis approach which uses conditional sampling to evaluate the noise contributions (see Ref.[7, 8, 20] for the conditional sampling procedures). This method does not require redundant signals used in some previous studies and the assumption (or

approximation) that the redundant signals are identical to the original signals. It does not rely on spectral analysis, allowing conditioning of the dissipation rate on the scalar value at the same location. The most important aspect of the method is the conditional sampling procedure, which is based on Kolmogorov's refined similarity hypotheses[21]. It is used to select fully resolved (verified a posteriori) local scalar fields, effectively separating the noise effects from the resolution effects. The fully resolved local scalar fields are then used to determine the measurement noise. Because the conditional sampling procedure makes use of the properties of turbulent scalar fields, it can essentially guarantee selection of fully resolved local scalar, even when the whole scalar field is not fully resolved. The experimentally determined noise is applied to potentially under-resolved conditional local scalar fields for noise correction.

We used the conditional sampling technique that we developed to study SGS scalar mixing[7, 8, 10, 22, 20, 15]. It uses two conditioning variables: the filtered (locally averaged) scalar. The technique makes use of the properties of the turbulent scalar fields. Our previous studies[7, 8, 10, 22, 20] have shown that for small SGS variance (smaller than mean SGS variance) the SGS scalar is well mixed. The statistics of such (conditional) fields are well described by the Kolmogorov-Obukhov-Corrsin theory. The locally averaged scalar dissipation rate and the scalar variance spectral transfer rate are lower than the mean scalar dissipation rate. In the spirit of the Kolmogorov's refined similarity hypotheses, the local conditional Peclet number is expected to be lower than that based on the unconditioned statistics. Therefore, the scalar dissipation length scales for these fields are expected to be larger than the mean scalar dissipation length scale. By choosing sufficiently small SGS variance values, one can select local scalar fields with large dissipation length scales so that they are well resolved by the measurement apparatus. This property of the local turbulent scalar fields is demonstrated by the experimental results (Fig. 11).

For large SGS variance, the locally averaged conditional scalar dissipation rate and the spectral transfer are larger than their mean values. In addition, the SGS scalar is highly segregated and contains the so-called ramp-cliff structure[9, 8, 10, 20]. The scalar dissipation rate is very large inside the cliffs. At the same time, the cliffs in the SGS scalar are likely to have smaller length scales. Using conditional sampling with large (much larger than the average SGS variance) SGS variance values, one can select local scalar fields that are potentially under-resolved to evaluate their dissipation length scales. These fields can be analyzed to determine the dissipation length scales and to correct for any under-resolution. Because this method makes use of the physics of the turbulent scalar fields, it does not require redundant measurements.

To obtain the scalar dissipation rate numerical (usually finite difference) schemes are needed to calculate the derivatives because experimental data are generally discrete samples. Different schemes involve different numbers of samples and different weights to the samples. Consequently,

the calculated scalar dissipation rate and the noise contribution are scheme dependent.

In this method we make use of the different spectral response (or resolution) of finite difference schemes (or numerical stencils) of different order in determining the measurement noise and evaluating the measurement resolution. Therefore, unlike some of the previous methods, this method does not rely on varying the measurement resolution (or the sample spacing) to evaluate dissipation length scale and only one resolution is needed.

In this study we used the assumption that the noises at different measurement locations (be it different samples from a single probe or pixels of an imaging device) are uncorrelated and are additive to the scalar values.

$$\xi = \xi^* + n \tag{8}$$

where $\xi^*$, $\xi$ and $n$ are the true scalar value, the measured value, and the noise, respectively. To correct for the noise contribution to the measured dissipation rate the noise variance needs to be determined.

For the Sandia flame data used in the present work, the measurement noise is dominated by shot noise. The mixture fraction was calculated using Bilger's formula with C and H elemental mass fractions. (Oxygen was excluded due to its high experimental uncertainty). All the major species mass fractions except CO were measured using Raman scattering. Due to the lower Raman signal/noise ratio these measured mass fractions have higher noise levels than the CO mass fraction measured by the two photon LIF technique. Therefore, the noise variance for the mixture fraction is dominated by the noise from the species measured by Raman scattering. Because the C and H atoms both originated from the fuel stream we expect the noise variance to increase with the mixture fraction. With this consideration we modeled the noise variance as proportional to the mixture fraction. Because the noise variance for the well resolved local scalar is determined near the stoichiometric mixture fraction, $\xi_s$, the model essentially evaluates the variations from that value. We have also tested a model that is locally constant with respective to the mixture fraction. The results show that the scalar dissipation length scales inferred using our approach are not sensitive to the details of the noise model, probably because the finite difference schemes involve samples with both lower and higher noise variances than that at the location where the derivative is calculated, partially cancelling the effects of the variations in the noise variance. Therefore, this simple model appears to be sufficiently accurate for the noise corrections.

To account for the dependence of the noise variance on the temperature we considered only the dependencies of the Raman scattering cross-sections on the mixture density but not on the the mixture compositions. Because the species number densities are proportional to the mixture density, so are the total scattering cross-section (signal) and the noise variance. Consequently, the

model noise variance for the normalized signal ($\xi$) is inversely proportional to the density and is proportional to the temperature for low-speed flows. The variance of noise is then modeled as proportional to both the mixture fraction and the temperature,

$$\langle n^2|\hat{\xi},\hat{T}\rangle = \sigma_n^2(\hat{\xi},\hat{T}) = B\cdot\xi^*\cdot T^* \tag{9}$$

By including this noise model in the finite difference scheme the measured derivative is

$$\begin{aligned} h\cdot\widetilde{\frac{d\xi}{dx}} &= a_1(\xi_1-\xi_{-1})+a_2(\xi_2-\xi_{-2})+a_3(\xi_3-\xi_{-3})+a_4(\xi_4-\xi_{-4})+\dots \\ &= a_1(\xi_1^*-\xi_{-1}^*)+a_2(\xi_2^*-\xi_{-2}^*)+a_3(\xi_3^*-\xi_{-3}^*)+a_4(\xi_4^*-\xi_{-4}^*)+\dots \\ &\quad + a_1n_1-a_{-1}n_{-1}+a_2n_2-a_{-2}n_{-2}+a_3n_3-a_{-3}n_{-3}+a_4n_4-a_{-4}n_{-4}+\dots \\ &= h\cdot\widetilde{\frac{d\xi^*}{dx}}+a_1n_1-a_{-1}n_{-1}+a_2n_2-a_{-2}n_{-2}+a_3n_3-a_{-3}n_{-3}+a_4n_4-a_{-4}n_{-4}+\dots \end{aligned} \tag{10}$$

where $\widetilde{\frac{d\xi^*}{dx}}$ is the estimated derivative without noise. Note that such an estimated derivative is dependent on the scheme used due to the different spectral responses. The measured mean dissipation rate is

$$\begin{aligned} \langle\tilde{\chi}\rangle &= \Big\langle 2D\Big(\widetilde{\frac{d\xi}{dx}}\Big)^2\Big\rangle \\ &= \Big\langle 2D\Big(\widetilde{\frac{d\xi^*}{dx}}\Big)^2\Big\rangle + \Big\langle\frac{2D}{h^2}\sum_{i=-N}^{N}a_i^2n_i^2\Big\rangle \\ &= \Big\langle 2D\Big(\widetilde{\frac{d\xi^*}{dx}}\Big)^2\Big\rangle + \frac{2\langle D\rangle}{h^2}\Big\langle\sum_{i=-N}^{N}a_i^2n_i^2\Big\rangle \\ &= \Big\langle 2D\Big(\widetilde{\frac{d\xi^*}{dx}}\Big)^2\Big\rangle + \frac{2\langle D\rangle}{h^2}B\sum_{i=-N}^{N}a_i^2\,\langle\xi_i^*T_i^*\rangle \\ &\approx \Big\langle 2D\Big(\widetilde{\frac{d\xi^*}{dx}}\Big)^2\Big\rangle + \frac{2\langle D\rangle}{h^2}B\sum_{i=-N}^{N}a_i^2\langle\xi_iT_i\rangle \end{aligned} \tag{11}$$

where $C_N=\sum_{i=-N}^{N}a_i^2\langle\xi_iT_i\rangle$, $D$, and $2D\Big(\widetilde{\frac{d\xi^*}{dx}}\Big)^2$ are a scheme dependent factor, the molecular diffusivity, and the estimated dissipation rate without noise, respectively.

When all the schemes can resolve the turbulence scalar field, the measured mean dissipation rate $\Big\langle 2D\Big(\widetilde{\frac{d\phi^*}{dx}}\Big)^2\Big\rangle$ does not depend on the scheme. Therefore, the measured mean dissipation rate vs. $C_N$ is a straight line with a slope of $\frac{2D}{h^2}\langle n^2\rangle$ and an intercept equal to the noise-corrected dissipation rate. This linear relationship can be used to determine the noise variance $\langle n^2\rangle$.

When the resolution is reduced, the measured dissipation rate obtained using the second-order scheme will first fall below the straight line because it is least capable of resolving the dissipation

rate. The deviation from the linear relationship will be followed by the fourth- and higher-order schemes as the resolution is further reduced. However, as long as the eighth- and tenth-order schemes follow this straight line the dissipation is still fully resolved. Therefore, the $\langle\chi\rangle - C_N$ plot can also be used to determine whether or not the scalar dissipation is fully resolved. In the following we employed the conditional sampling method to select fully resolved local scalar fields and determine the noise variance according to Eq. 9. The noise variance was then used to correct the dissipation rate from potentially under-resolved local scalar fields. The noise-corrected dissipation rates from the different schemes were then analyzed to evaluate the scalar dissipation length scales and to correct for the resolution effects.

In this study we used the Favre filtered (locally averaged) scalar and the Favre SGS scalar variance as conditioning variables. The conditionally filtered dissipation rates were calculated using five central difference schemes. As the scheme order increased, the conditionally filtered dissipation rates increased. Figure 11 shows that in Flame D at $x/D = 15$ for $\langle\xi\rangle_L = 0.35$ and $\langle\xi''^2\rangle_L = 5.2 \times 10^{-4}$ (small SGS variance), the $\langle\langle\chi|\xi\rangle|\langle\xi\rangle_L, \langle\xi''^2\rangle_L\rangle - C_N$ plot forms a straight line, indicating that for small SGS variance, the scalar fields were well resolved by all the schemes. Note that the noise-corrected conditionally filtered dissipation (the intercept) is of the same order as the noise contributions, indicating that the method is capable of accurately determining the noise variance even when the noise contribution was larger than the true dissipation rate.

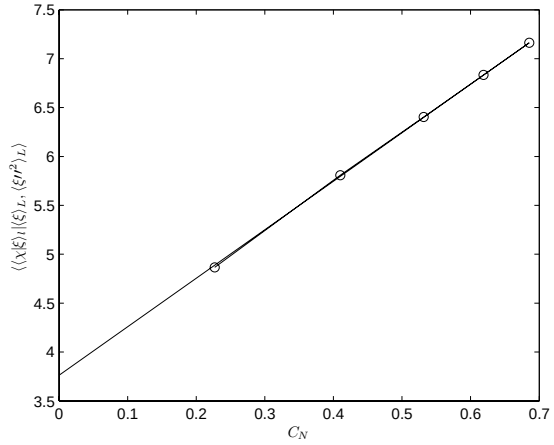


Figure 11: Dissipation rates vs $C_N$ in D15, $\langle\xi''^2\rangle_L = 5.2 \times 10^{-4}$

From Fig. 11 the noise variance and $B$ in Eq. 9 can be determined for flame D at $x/D = 15$. For small SGS variance values the fluctuations in both the mixture fraction and the temperature were small, therefore the noise evaluation for the well-resolved scalar fields does not depend on the specific noise model used as long as the noise variance is a function of the mixture fraction and the

temperature.

For large SGS variance, $\langle \xi''^2 \rangle_L = 6.7 \times 10^{-2}$ (Fig. 12), the conditionally filtered dissipation rates using the sixth- and lower-order schemes are below the straight line formed by the eighth- and tenth-order schemes, indicating that the sixth- and lower-order schemes were not capable of resolving all the scalar length scales. Note that the dissipation rate using the second-order scheme ($\sim 139 s^{-1}$) is less than the intercept of straight line ($\sim 148.7 s^{-1}$), indicating that even without correcting for noise the second-order scheme is underestimating the dissipation rate. However, there is no evidence to show that whether eighth and tenth order schemes are capable of fully resolving the scalar scales. Therefore, the true dissipation is equal or higher than the intercept of the straight line.

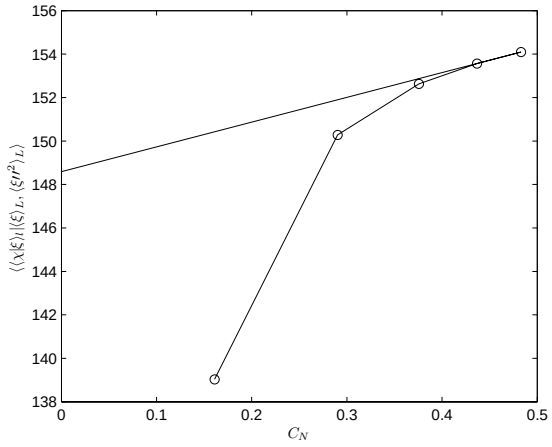


Figure 12: Dissipation rates vs $C_N$ in D15, $\langle \xi''^2 \rangle_L = 6.7 \times 10^{-2}$

The conditionally filtered dissipation rates conditioning on mixture fraction using schemes of different orders at two SGS scalar variances $\langle \xi''^2 \rangle_L = 5.2 \times 10^{-4}$ and $6.7 \times 10^{-2}$ are given in Figs. 13a and 14a respectively. The figures show that the calculated dissipation rates increase as the order of schemes increases. The increases come from both noise and better resolution of the higher-order schemes. We subtracted the noise contributions determined above from the dissipation rate. The results are given in Figure 13b and 14b.

For small SGS scalar variance ($\langle \xi''^2 \rangle_L = 5.2 \times 10^{-4}$, Figure 13), the corrected dissipation rates calculated using second- to tenth-order schemes largely overlap, indicating that all the schemes were sufficient to resolve the scalar dissipation length scales and the noise contributions had been removed. For large SGS scalar variance ($\langle \xi''^2 \rangle_L = 6.7 \times 10^{-2}$, Fig. 14), the conditionally filtered dissipation rates for different schemes are closer after the noise correction. Lower-order schemes still give lower dissipation rates. The increase of the calculated dissipation rate from the second-order

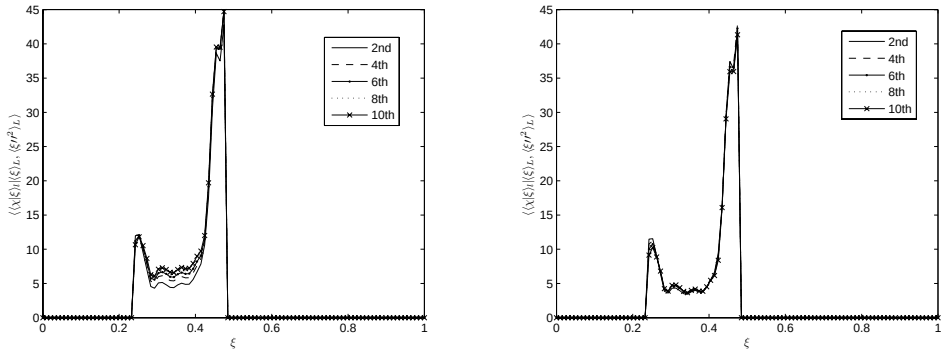


(a) Before noise correction (b) After noise correction

Figure 13: Conditionally filtered dissipation rates before and after noise correction in D15, $\langle \xi''^2 \rangle_L = 5.2 \times 10^{-4}$

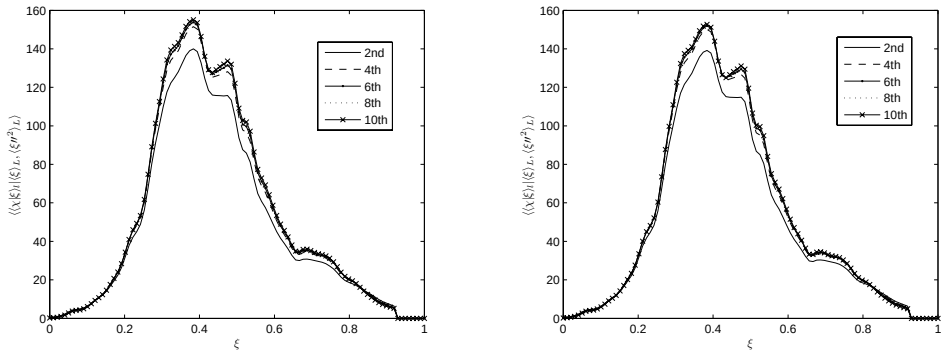


(a) Before noise correction (b) After noise correction

Figure 14: Conditionally filtered dissipation rates before and after noise correction in D15, $\langle \xi''^2 \rangle_L = 6.7 \times 10^{-2}$

to fourth-order is large, indicating that the second-order scheme was far from having sufficient resolution. The differences between the eighth- and tenth-order schemes are much smaller, indicating dissipation rates calculated using these schemes are close to the true dissipation rate. Note that the noise contributions are close to $3 \sim 5\text{s}^{-1}$ regardless of the SGS variance. Therefore, the relative amount of correction is smaller for large SGS variance.

After correcting for the noise, the measured dissipation rate is only affected by the resolution, which is expected to be the worst when the SGS scalar variance is large due to the sharp cliffs in the SGS scalar. Because the scalar dissipation length scales were not known *a priori*, we needed to use experimental data to infer them. Comparing the measured scalar spectrum to a model spectrum can provide an estimate of the average length scale, but not that of the cliffs, which dominate the scalar dissipation rate for large SGS variance. To estimate the the length scales of the cliffs we

used the error function as a model for the ramp-cliff structure in the SGS scalar field and calculate the dissipation rate using different schemes with a range of sample intervals (spatial resolutions).

We used the ratios of the dissipation rates calculated using different schemes to infer the scalar dissipation scales. By equating the ratios from the measured dissipation rates and from the model, a scalar dissipation scale was inferred. The ratios of dissipation rates are shown in Figure 15. Here the ratios for the highest dissipation rate (at $\xi = 0.5$) are shown in Fig. 15 and are compared with the error-function model because these ratios correspond to the smallest scalar length scale. The horizontal axis is the ratio of sample distance to the scalar profile width, $h/w$. The ratio of the second-order to the tenth-order estimations is approximately 0.84, giving a $h/w$ of 0.52. The scales inferred from all the other schemes also agree very well, indicating the overall success of the noise correction and resolution/length scale evaluation. At this sample interval $h/w = 0.52$ figure 16 shows that the second-order scheme under-estimated the dissipation rate by 16%, the sixth-order scheme by 2%, the eighth- and tenth-order by less than 1%. Therefore, a sample interval of approximately 0.5 $w$ is sufficient to resolve the dissipation rate.

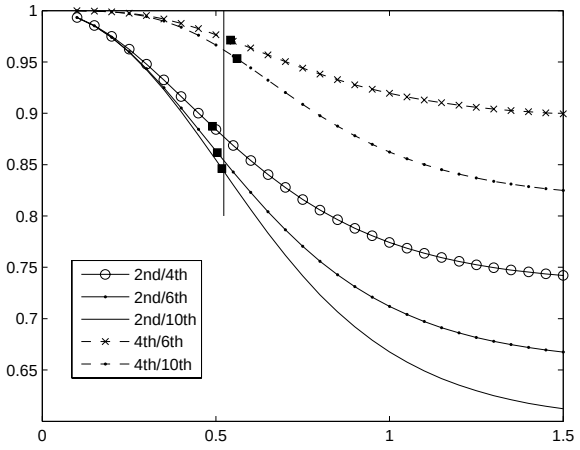


Figure 15: Estimation of scale by comparing the ratio of dissipation rates from the data and model. Ratio of dissipation rates using different schemes is plotted as curve. Solid squares are calculated from the data.

The resolution correction considered here are for large SGS variance, corresponding to the largest dissipation rate. The method in the present study can be applied to the mean scalar dissipation rate by summing the corrected dissipation rate for each SGS variance values weighed by the probability for each SGS variance value. Because the resolution improved with decreasing SGS variance, the percentage of the resolved mean dissipation is expected to be higher. Therefore, the amount of correction for the mean dissipation rate will be smaller.

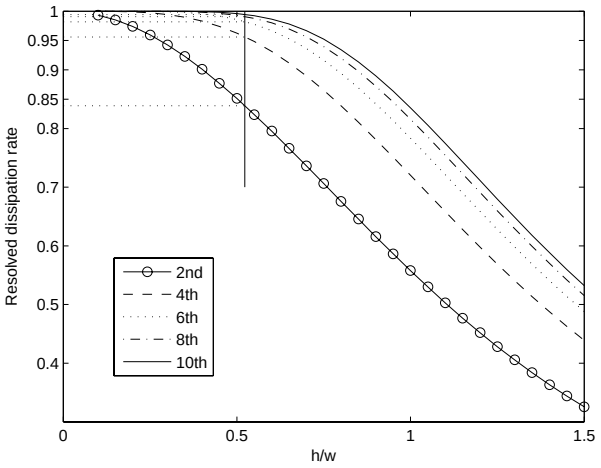


Figure 16: Estimation of resolved dissipation rates using the error function model.

# IV Conclusions and suggestions for LES

The results obtained in this research significantly advanced the understanding of the SGS mixing of the mixture fraction (a conserved scalar) and temperature (a reactive scalar), which is important for modeling SGS mixing in LES of turbulent combustion. The issues investigated include the scalar FMDF and its transport equation, the scalar-temperature FMDF and the FMDF transport equation. We also developed and tested a conditional-sampling-based method for noise and resolution corrections for scalar dissipation rate measurements. The specific conclusions and suggestions for LES are:

- The mixture fraction FMDF is unimodal for small SGS scalar variance regardless of the filter scale. The conditionally filtered scalar dissipation rate depends weakly on the SGS scalar, indicating that the SGS scalar is well mixed. Therefore, such a SGS mixture fraction is likely to result in distributed reaction zones.

- For large SGS variance the FMDF becomes bimodal and the conditionally filtered scalar dissipation is bell-shaped, indicating the existence of a ramp-cliff structure, which is similar to the mixture fraction profile in the counter-flow model for laminar flamelets. Therefore the SGS mixing field under such conditions support flamelets.

- At a given location the SGS flame fluctuated between distributed reaction zones and laminar flamelets in the flames studied. Laminar flamelets contributed to nearly 50% of the heat release, further highlighting its importance in flames and the need for mixing models to capture the bimodal FMDF.

- The mixture-fraction-temperature FMDF also has qualitatively different shapes for small and large SGS variance. For small SGS variance the FMDF is unimodal but for large SGS variance it is bimodal with the two peaks outside of the reaction zone.

- The conditionally filtered mixture fraction dissipation for small SGS variances is generally consistent with quasi-equilibrium distributed reaction zones with a relatively weak dependence on the mixture fraction. For the extinguished samples it is not very large and is not sensitive to the temperature, suggesting that these may be samples extinguished at some upstream locations.

- For large SGS variance, the dissipation is large near $\xi = 0.4$, where the maximum gradient in a cliff is located. The dissipation is higher for lower temperatures, consistent with strained laminar flamelets. For the extinguished samples, the measured dissipation rate component exceeds the extinction dissipation rate. The results indicate that these were extinguished flamelets.

- The conditionally filtered temperature dissipation for small SGS variances has a minimum (close to zero) near the peak temperature. For the extinguished samples with very low temperatures ($< 1300K$), the dissipation is lower compared to those with intermediate temperatures ($1300 - 1600K$). The latter is due to the mixing between burning and very low temperature samples. Therefore, the mixture fraction was well mixed but temperature was not.

- For large SGS variance, the dissipation indicates strained or extinguished laminar flamelets. However, the pilot flame played an important role. For samples not far from equilibrium, the dissipation is consistent with strained laminar flamelets. Further away from equilibrium at moderate temperature (as high as 1700K) there are dissipation peaks which are probably a result of the rapid mixing between the pilot gas and the lean or rich mixtures, corresponding to extinguished flamelets.

- The conditional-sampling-based noise and resolution corrections for scalar dissipation rate measurements can guarantee selection of well resolved local scalar fields to accurately determine the noise variance and remove the noise contribution. The conditional sampling procedure combined with the ramp-cliff model enables accurate determination of the dissipation length scale and correction for under-resolution.

In collaboration with Professors Pope and Givi we are currently working on testing models and LES predictions (FMDF, etc.) and are exploring the possibilities of using the above results to improve models. In particular the issue of the ability of mixing models to predict the very

different SGS mixing characteristics of conserved scalars (mixture fraction) and reactive scalars (temperature) will be explored.

## References


[1] S. B. Pope, "Computations of turbulent combustion: Progress and challenges," in *Proceedings of the 23rd Symposium (International) on Combustion* (1990), pp. 591–612.

[2] L. Y. M. Gicquel, P. Givi, F. A. Jaberi, and S. B. Pope, "Velocity filtered density function for large eddy simulation of turbulent flows," Phys. Fluids **14,** 1196–1213 (2002).

[3] M. R. H. Sheikhi, T. G. Drozda, P. Givi, and S. B. Pope, "Velocity-scalar filtered density function for large eddy simulation of turbulent flows," Phys. Fluids **15,** 2321–2337 (2003).

[4] R. S. Barlow and A. N. Karpetis, "Measurements of scalar variance, scalar dissipation, and length scales in turbulent piolted methane/air jet flames," Flow, Turb. Combust. **72,** 427–448 (2004).

[5] A. N. Karpetis and R. S. Barlow, "Measurements of flame orientation and scalar dissipation in turbulent partially premixed methane flames," Proc. Combust. Inst. **30,** 665–672 (2005).

[6] R. S. Barlow and A. N. Karpetis, "Scalar length scales and spatial averaging effects in turbulent piloted methane/air jet flames," Proc. Combust. Inst. **30,** 673–680 (2005).

[7] C. Tong, "Measurements of conserved scalar filtered density function in a turbulent jet," Phys. Fluids **13,** 2923–2937 (2001).

[8] D. Wang and C. Tong, "Conditionally filtered scalar dissipation, scalar diffusion, and velocity in a turbulent jet," Phys. Fluids **14,** 2170–2185 (2002).

[9] C. Tong and Z. Warhaft, "On passive scalar derivative statistics in grid turbulence," Phys. Fluids **6,** 2165–2176 (1994).

[10] A. G. Rajagopalan and C. Tong, "Experimental investigation of scalar-scalar-dissipation filtered joint density function and its transport equation," Phys. Fluids **15,** 227–244 (2003).

[11] J. H. Frank, S. A. Kaiser, and M. B. Long, "Reaction rate, mixture fraction, and temperature imaging in turbulent methane/air jet flames," Proc. Combust. Inst. **29,** 2687–2694 (2002).

[12] E. S. Bish and W. J. A. Dahm, "Strained dissipation and reaction layer analysis of nonequilibrium chemistry in turbulent reacting flows," Combust. Flame **100,** 457–464 (1995).

[13] D. Wang, Ph.D. dissertation, Clemson University, Department of Mechanical Engineering, 2005.

[14] A. N. Karpetis and R. S. Barlow, "Measurements of scalar dissipation in turbulent piloted methane/air jet flames," Proc. Combust. Inst. **29,** 1929–1936 (2002).

[15] D. Wang, C. Tong, R. S. Barlow, and A. N. Karpetis, "Experimental study of scalar filtered mass density function in turbulent partially premixed flames," Proc. Combust. Inst. **31,** 1533–1541 (2007).

[16] R. W. Bilger, "The structure of turbulent nonpremixed flames," in *Proceedings of the Twenty-Second Symposium (International) on Combustion* (1988), pp. 475–488.

[17] P. Sripakagorn, S. Mitarai, G. Kosaly, and H. Pitsch, "Extinction and reignition in a diffusion flame: a direct numerical simulation study," J. Fluid Mech. **518,** 231–259 (2004).

[18] S. Mitarai, S. M. de Bruyn Kops, and C. M. Cha, "Direct numerical simulations of the double scalar mixing layer Part II: Reactive scalars," Combust. Flame **149,** 392–408 (2007).

[19] H. Pitsch and H. Steiner, "Scalar mixing and dissipation rate in large-eddy simulations of non-premixed turbulent combustion," in *Proc. Combust. Inst.* (2000), pp. 41–49.

[20] D. Wang and C. Tong, "Experimental study of velocity-scalar filtered joint density function for LES of turbulent combustion," Proc. Combust. Inst. **30,** 567–574 (2005).

[21] A. N. Kolmogorov, "A refinement of previous hypothesis concerning the local structure of turbulence in a viscous incompressible fluid at high Reynolds number," J. Fluid Mech. **13,** 82–85 (1962).

[22] D. Wang, C. Tong, and S. B. Pope, "Experimental study of velocity filtered joint density function and its transport equation," Phys. Fluids **16,** 3599–3613 (2004).

## Publications resulted from this research


1. Wang, D., Tong, C., Barlow, R.S., and Karpetis, A.N. 2007 Experimental study of scalar filtered mass density function in turbulent partially premixed flames. *Proc. Combust. Inst.* **31**, 1533–1541.

2. Cai, J., Wang, D., Tong, C., Barlow, R.S., and Karpetis, A.N. 2009 Investigation of subgrid-scale mixing of mixture fraction and temperature in turbulent partially premixed flames. *Proc. Combust. Inst.* **32**, 1517–1525.

3. Cai, J. and Tong, C. 2008 A conditional-sampling-based method for noise and resolution corrections for scalar dissipation rate measurements. Submitted to *Phys. Fluids*. (Revision under review.)

**Presentations on the results from this research**

1. Investigation of subgrid-scale mixing of mixture fraction and temperature in turbulent partially premixed flames. The thirty second International Symposium on Combustion. Montreal, 2008

2. Subgrid-scale scalar diffusion in turbulent partially premixed flames 60th Annual Meeting of the Division of Fluid Dynamics of the American Physical Society. Salt Lake City, 2007.

3. Experimental study of scalar filtered density function and scalar dissipation rate. Institute of Combustion Technology. University of Aachen, Germany. June 2007

4. Investigation of subgrid-scale mixing and turbulence-chemistry interaction in turbulent partially premixed flames using experimental data. Institute of Combustion Technology. University of Aachen, Germany. June 2007

5. Effects of the subgrid-scale mixture fraction structure on scalar and temperature dissipation in turbulent partially premixed flames. 5th US national Meeting on Combustion. San Diego, 2007

6. Experimental study of subgrid-scale turbulent mixing and turbulence-chemistry interaction. Department of Mechanical Engineering, University of Wyoming. 2007.

7. Experimental study of scalar filtered mass density function in turbulent partially premixed flames. The thirty first International Symposium on Combustion. Heidelberg, Germany, 2006

## Participating Personnel

Chenning Tong: Associate Professor (11/15/2005-11/14/2008)

Jian Cai: Graduate student (11/15/2005-11/14/2008)

### Interactions with researchers at AFRL

During the period of this grant, The PI continued the collaboration with Dr. Campbell Carter. In 2004 the PI initiated contacts with several researchers at AFRL to seek opportunities for collaborations. The discussions with Dr. Carter resulted in a collaborative project. In the summers of 2005 and 2006 the PI spent several weeks at AFRL as part of the collaboration.

This collaboration focuses primarily on issues of using measurements to improve of large eddy simulation (LES) of nonpremixed turbulent combustion. In PDF-based LES approaches the subgrid-scale mixing of multiple scalars must be modeled. Current mixing models are based primarily on knowledge gained from two-stream mixing problems (e.g., fuel mixing with oxidizer). However, in a reacting flow at least three scalars are involved (the third is a product). Therefore, understanding of three-stream SGS mixing is important for modeling mixing in nonpremixed turbulent combustion. As a step toward understanding SGS mixing of multiple reactive scalars, the PI and Dr. Carter are studying the SGS mixing in a three-stream non-reacting jet. The jet nozzle consists of an axisymmetric jet and an annulus from which acetone-doped air and ethylene are issued into an air co-flow. Laser diagnostics (planar laser induced fluorescence and Rayleigh scattering) were employed to obtain images of the species. The PI is currently analyzing the data. This study will provide a basis for future investigations of multi-scalar SGS mixing in turbulent flames.

## Inventions

None